Article

Anaerobic Digestion of the Organic Fraction of Municipal Solid Waste in Plug-Flow Reactors: Focus on Bacterial Community Metabolic Pathways

Elena Rossi [1] , Simone Becarelli [2] , Isabella Pecorini [1,*] , Simona Di Gregorio [2] and Renato Iannelli [1]

[1] Department of Energy, Systems Territory and Construction Engineering, University of Pisa, 56122 Pisa, Italy; elena.rossi@phd.unipi.it (E.R.); renato.iannelli@unipi.it (R.I.)
[2] Department of Biology, University of Pisa, 56122 Pisa, Italy; simone.becarelli@biologia.unipi.it (S.B.); simona.digregorio@unipi.it (S.D.G.)
[*] Correspondence: isabella.pecorini@unipi.it

Abstract: The aim of this study is to investigate the performance of a pilot-scale plug-flow reactor (PFR) as a biorefinery system to recover chemicals (i.e., volatile fatty acids (VFAs)), and biogas during the dry thermophilic anaerobic digestion (AD) of the organic fraction of municipal solid waste (OFMSW). The effects of the hydraulic retention time (HRT) on both outputs were studied, reducing the parameter from 22 to 16 days. In addition, VFA variation along the PFR was also evaluated to identify a section for a further valorization of VFA-rich digestate stream. A particular focus was dedicated for characterizing the community responsible for the production of VFAs during hydrolysis and acidogenesis. The VFA concentration reached 4421.8 mg/L in a section located before the end of the PFR when the HRT was set to 16 days. Meanwhile, biogas production achieved 145 NLbiogas/d, increasing 2.7 times when compared to the lowest HRT tested. *Defluviitoga* sp. was the most abundant bacterial genus, contributing to 72.7% of the overall bacterial population. The genus is responsible for the hydrolysis of complex polysaccharides at the inlet and outlet sections since a bimodal distribution of the genus was found. The central zone of the reactor was distinctly characterized by protein degradation, following the same trend of propionate production.

Keywords: anaerobic digestion; *Defluviitoga* sp. plug-flow reactor; bacterial metabarcoding; functional metagenomic prediction; VFA

1. Introduction

The most recent European policies address the valorization of biowaste towards the fulfillment of circular economy [1] and bioeconomy [2] principles. Despite that the European waste hierarchy has food waste prevention at the top, food waste still accounts for 60% of the biowaste currently generated in the European Union (EU). In addition, the Waste Framework Directive (WFD) [3] imposes rules to separately collect food waste by the end of 2023. Meanwhile, a landfill directive has reduced the quantity of municipal solid waste (MSW) landfilled to 10% [4]. Considering both actions, it appears that the separately collected organic fraction of municipal solid waste (OFMSW) is a continuously increasing waste stream.

In this frame, many efforts were made to provide proper management of OFMSW. Recent experimental studies found that OFMSW is a proper carbon source for biorefinery systems due to its bromatological, physical–chemical, and elemental composition [5]. Anaerobic digestion (AD) of OFMSW is an example of biorefinery catalyzed by the bacterial community, capable of transforming biodegradable compounds into by-products, e.g., converting OFMSW in both high-volume but low-value products (i.e., biogas, biofuels, heat electricity) and high-value but low-volume products (i.e., chemicals as fertilizers and volatile fatty acids (VFAs)) [6]. In detail, VFAs are organic compounds (e.g., C2–C6; namely,

acetic, propionic, butyric, iso-butyric, valeric, iso-valeric, and caproic acids) with broad applicability in the current industry sector as chemical building blocks [7]. Currently, the demand for peculiar VFAs is dramatically increasing. However, their production relies mainly on the chemical synthesis of non-renewable sources, resulting in huge environmental impacts. To reduce this criticality, microbial production of VFAs by AD of OFMSW is raising attention since it uses low-value compounds and is free of several environmental issues.

So far, wet processes, in which the total solid (TS) content in the digester is lower than 5%, prevail compared to dry processes in which the TS content ranges between 20–40%. Wet AD ensures a homogenous distribution of feedstock and seed-sludges, along with the availability of easy biodegradable organic matter in the digester, thus resulting in great specific biogas production (SGP) [8] as well as VFAs. However, the continuous mixing requires high energy consumption, solid organic waste (i.e., such as OFMSW) needs the addition of a large amount of water to maintain TS < 10%, and the handling of digested sludges requires costly dewatering processes [9]. On the contrary, dry AD can treat solid organic waste with little or no water addition without requiring any continuous mixing. Furthermore, dry AD can handle higher organic loading rates (OLRs) with smaller reactor volumes than wet AD. For these reasons, dry AD plants are expected to rapidly increase in the following years [10]. In this context, plug-flow reactors (PFRs) represent one of the technologies conventionally applied [11]. Specifically, PFRs have a rectangular shape as a distinctive feature. The entrance of new feedstock, together with the withdrawal of digestate, allows the horizontal movement of the feedstock from the inlet to the outlet without any mixing along the longitudinal direction.

In the past, most of the studies focused on optimizing biogas production using PFRs. For example, Zeshan et al. [12] found that a C/N ratio of 32 is optimal to avoid ammonia inhibition. Several authors studied the effects of the organic loading rate (OLR) on biogas production. For instance, Jabeen et al. [13] found an inverse relationship between OLR and SGP during the mesophilic co-digestion of food waste and rice husk, and an analogous result was found by Patinvoh et al. [14] during the co-digestion of manure and straw. However, in the context of AD biorefinery, operating conditions of PFRs can also be optimized to enhance the production of VFAs.

Currently, most of the studies investigating the effects of operating parameters on VFA productivity are batch tests at the laboratory scale level. For example, alkaline conditions increase VFA concentration during fermentation of OFMSW at both thermophilic and mesophilic temperature (i.e., 8000 and 7000 mgCOD/L, respectively) [15], while a recent study found that alkaline pH increases the share of acetic acid; Slezak et al., [16] found a positive correlation between OLR and VFA concentrations since the authors obtained a maximum concentration (above 10 g/L) for OLR of 48.2 gVS/L. Among the few pilot-scale tests, two-stage configuration systems are mainly studied as biorefinery platforms. In this regard, two continuously stirred tank reactors (CSTRs), placed in series, obtained a VFA yield ranging from 0.18 to 0.32 $kgCOD_{VFA}/kgCOD_{IN}$ when they operated at thermophilic conditions with an OLR of 17 and 19 gVS/(L d), respectively. Nevertheless, these systems can present a critical drop of pH (<5) in the first reactor, thus needing chemical dosage or automatic control systems to recirculate digestate from the methanogenic to acidogenic reactors. In addition, a great amount of process water is needed in the case of OFMSW since this configuration only allows wet processes. As a consequence, VFA production in PFRs from AD of OFMSW is scarcely addressed. In addition, information on the variability of VFA concentration and composition along the digester is lacking as well. However, this information is crucial to understanding where VFA production is maximized, thus indicating a possible section to partially remove digestate for further applications (e.g., production of polyhydroxyalkanoates (PHA)).

From a microbiological point of view, during AD, four sequential steps occur, involving at least three groups of microbial communities [17]. Firstly, organic matter (e.g., carbohydrates, proteins, and fats) is hydrolyzed in monomers (e.g., sugar, amino acids, and fatty acids) by hydrolytic bacteria mainly belonging to Bacteroidetes and Firmicutes;

successively, in the acidogenic step, monomers are mainly converted in VFAs, hydrogen (H_2), carbon dioxide (CO_2), and ethanol by the so-called acid-former bacteria, belonging mainly to Bacteroidetes, Chloroflexi, Firmicutes, and Proteobacteria; finally, acetate and H_2 are converted in methane (CH_4) and CO_2 by methanogenic Archaea. Changing the process operating conditions (i.e., temperature, pH, hydraulic retention time (HRT), OLR, TS content), substrate, and pretreatments can induce significant changes in the microbial ecology of the system, with shifts in the dominating metabolic pathways and changes in the concentration, composition, and yield of intermediates, i.e., VFAs [5] as well as final products, i.e., biogas [15–17]. A literature review highlighted, in detail, that *Firmicutes* produce butyrate, especially for high OLR [16]; at pH = 10, the *Ruminococcaceae* family was found to be strongly and positively correlated with butyric acid production (initial pH = 10) [18]. In contrast, acetic acid production seems to be primarily performed by the *Bacteroidetes* phylum [16], but Khatami et al. [18] found a positive correlation with *Veillonellaceae*, and *Lactobacillaceae* families, members of phylum *Firmicutes*, when pH was set to 5. It is worth mentioning that despite their exploitation, PFRs are scarcely studied with regard to microbial ecology and VFA production. To the best of the authors' knowledge, only one recent study has investigated the relationship between AD performance, microbial ecology, and operating conditions in PFR. However, referring to that study, the objective was to link the effect of the recirculation ratio on the microbial ecology of a reactor to achieve optimal biogas production without studying VFA production [19].

The aim of this study is to provide an insight into VFA production in a pilot-scale PFR during dry thermophilic AD of OFMSW when HRT varies, with a focus on the bacterial ecology responsible for the successive stages of the VFA production: hydrolysis and acidogenesis. To this aim, a metabarcoding approach was adopted in parallel to predictive functional metagenomic analysis to infer the bacterial groups putatively involved in the different phases of the process.

2. Materials and Methods

2.1. Pilot Scale Plug-Flow Reactor

A pilot-scale AISI 316 stainless steel PFR with an effective volume of around 37 L was used in the experimental test. Figure 1 illustrates a schematic representation of the pilot-scale digester. At the inlet, a gas-tight cylinder and a piston ensure the feeding of the digester without any gas escaping. The substrate moves inside the digester from the inlet to the outlet thanks to the daily feeding, while an internal mixing system made of blades homogenizes the substrate and digestate along the cross-section of the reactor. The digestate was daily removed through a 2″ ball valve and partially recirculated (see Section 2.3). A water jacket surrounded the digester to maintain thermophilic conditions (55 ± 2 °C). The water was heated in a tank using a thermostat heater (FA 90, Falc Instruments Srl, Treviglio (BG), Italy); meanwhile, a centrifuge hydraulic pump (PQm 90, Pedrollo SpA, San Bonifacio (VR), Italy) recirculated the water from the tank to the water jacket. The production of biogas was continuously measured by means of a volumetric counter whose functioning was previously described in Baldi et al., [20]. An infrared sensor (Gascard NG, Edinburgh Sensors, Livingston EH54 7DQ, UK) continuously measured the composition of biogas in terms of CH_4 and CO_2. Two probes (InPro 4281i, Mettler-Toledo SpA, Milano (MI), Italy) continuously measured pH and temperature of the digestate at two intermediate sections of the digester (i.e., pH1 and T1 for the probe near to the inlet, pH2 and T2 for the probe near to the outlet). Ambient temperature and atmospheric pressure were measured using a Pt 100 sensor (THERMASGARD® ATM 2, S+S Regeltechnik GmbH, Nürnberg, Germany) and a pressure transmitter (PREMASGARD®ALD, S+S Regeltechnik GmbH, Nürnberg, Germany), respectively. The signals coming from the sensors were acquired by a cRIO 9030 controller (National Instruments, Austin, TX, USA) and were processed by software specifically developed in the LabVIEW® 2017 environment.
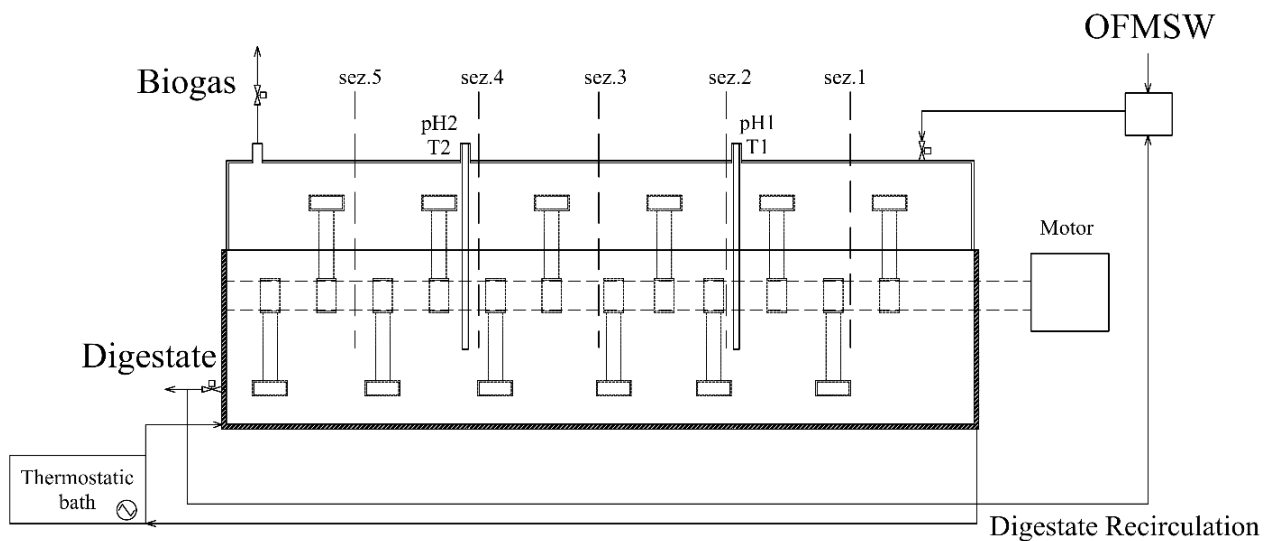
Figure 1. Schematic view of plug-flow reactor (PFR) and digestate sampling sections (sez.1–sez.5).

Finally, Figure 1 illustrates the five sections where the digestate was sampled to understand the trend of VFA production along the PFR. Further details on the sampling campaigns are described in Section 2.3.

2.2. Substrate and Inoculum

A sample around of 260 kg of OFMSW was collected from a door-to-door collection system in the municipality of Florence, Italy. Initially, the sample was sieved throughout a star screen at 80 mm, then manually sorted to remove inert and undesirable materials and plastics. Finally, OFMSW was shredded in a meat grinder (DVM 3040, Hudson Mesa Srl, San Giorgio su Legnano (MI), Italy) and stored in a freezer at $-20\,^\circ$C in plastic tanks to prevent further biodegradation. In this study, the seed sludge was a dry thermophilic digestate collected from a full-scale anaerobic digester treating OFMSW and garden waste (GW).

2.3. Experimental Design

The PFR operated for an overall period of 150 days. At the beginning of the test, the seed sludges were maintained at thermophilic conditions without feeding for 10 days to degrade the residual organic matter (i.e., degassing phase) [21]. Then, the feeding period started. The pilot-scale PFR was manually fed every working day, thus operating semi-continuously. Furthermore, when the PFR was fed, an equal flow of digestate was withdrawn to operate the system in a stationary mode.

The inlet volumetric flow of OFMSW ($Q_{OFMSW} - L/d$) was inoculated with the digestate, taken from the outlet section before feeding operations started. The amount of digestate used as inoculum, namely, Q_r (L/d), was calculated from Q_{OFMSW} by fixing a recirculation ratio (i.e., $\alpha = Q_r/Q_{OFMSW}$) of 0.45. Then, Q_r was manually mixed with Q_{OFMSW}. Finally, by means of a piston and a cylinder sealed with a locking nut to avoid any gas escape, OFMSW was manually fed to the reactor.

The experimental tests were characterized by three scenarios with different HRTs. The HRT was changed by modifying Q_{OFMWS} since the reactor working volume (W_V) was fixed at 28 L. Firstly, the HRT was set to 22 days (S1), then it was reduced to 19 days (S2); finally, it was decreased to 16 days (S3). These values were chosen because they are those commonly applied in full-scale dry AD plants [9,22], thus being optimal towards a scale-up of the process.

As a consequence, the inlet volumetric flow (Q_{in}) was calculated by Equation (1) [23]:

$$HRT = W_V/Q_{in} \tag{1}$$

where Q_{in} (L/d) is the sum of Q_{OFMSW} (L/d) and Q_r (L/d). For each HRT, a corresponding OLR was computed, as follows, using Equation (2):

$$OLR = Q_{VS}/W_V \qquad (2)$$

where Q_{VS} (gVS/d) is the daily mass of volatile solid (VS) that is calculated by multiplying Q_{OFMSW} (g/d) by the VS content of the inlet OFMSW (see Table 1). In the calculations, 0.92 g/mL was used as bulk density of OFMSW to convert mass flows into volumetric flows. As a result, OLR was 6. 4, 8.4, and 12.7 gVS/(L d) for S1, S2, and S3, respectively.

Table 1. Feedstock and inoculum characteristics.

Parameter °	T1	T2	T3	T4	T5
C/N [-]	26.05 ± 2.6	18.08 ± 1.8	18.08 ± 1.8	19.19 ± 1.91	32.02 ± 3.2
Carbohydrates [%VS]	44.63 ± 4.24	33.75 ± 3.2	33.75 ± 3.2	25.96 ± 2.46	46.95 ± 4.46
Proteins [%VS]	13.52 ± 1.55	16.98 ± 1.95	16.98 ± 1.95	10.04 ± 1.15	14.41 ± 1.65
Lipid [%VS] [%VS]	1.51 ± 0.13	1.85 ± 0.16	1.85 ± 0.16	0.84 ± 0.07	1.74 ± 0.15
Lignin [%VS]	24.84 ± 2.73	19.81 ± 2.17	19.81 ± 2.17	16 ± 1.76	13.99 ± 1.53
Cellulose [%VS]	13.1 ± 1.04	18.43 ± 1.47	18.43 ± 1.47	8.83 ± 0.7	23.05 ± 1.84

° $n = 2$.

To study the concentration and the composition of VFAs along the PFR, five sampling campaigns were conducted. After the degassing phase, digestate was sampled monthly, thus resulting in five samples identified as T1, T2, T3, T4, and T5. In detail, T1 was sampled during S1, T2 and T3 were collected during S2, while T4 and T5 belong to S3. Finally, sampling was performed using a customized probe to avoid any contamination with the digestate in the adjacent sections.

2.4. Analytical Methods

The inlet substrate and the outlet digestate were characterized daily for TS, VS, and pH. The digestate was also characterized in terms of alkalinity, total ammonia nitrogen (TAN), free ammonia (FA) concentration, and total and specific VFA concentration on a daily basis. In addition, the concentration of total and specific VFAs was measured on the digestate sampled from sections sez.1–sez.5 (Figure 1).

TS and VS were measured gravimetrically: firstly, the samples were dried at 105 °C for 24 h and then burned at 550 °C for 6 h. pH was measured using a pH-meter (pH 7 + DH2, XS Instruments, Carpi, MO, Italy), mixing a ratio of 10 g of sample to 100 mL of deionized water in accordance with [24].

Alkalinity, TAN, and FA were measured on the liquid part of the digestate after centrifugation at 13,500 rpm for 20 min. Alkalinity was measured on unfiltered supernatant through two-endpoints titration, which was done using 1 M hydrochloric acid (HCl). The endpoints were at pH = 5.75 for the titration of bicarbonate (partial alkalinity, PA) and at pH = 4.3 for the titration of organic acids (total alkalinity, TA) [25]. Intermediate alkalinity (IA), which is generally associated with the organic acids within the digestate, was then calculated as the difference between TA and PA. The ratio IA/PA was used to monitor process stability as it is applied in conventional full-scale biogas plants [26]. To measure TAN, the supernatant was firstly diluted with deionized water on a volumetric ratio of 1:500, and then the concentration was measured using an ammonia medium-range reagent kit (HI93715-03, Hanna Instrument, Ronchi di Villafranca Padovana, Italy) and a photometer (HI 83099, Hanna Instrument, Ronchi di Villafranca Padovana, Italy). Consequently, FA was calculated through the equation reported by Rajagopal et al. [27] using the TAN concentration (evaluated as described above) and the pH and temperature measured at the sampling date.

The macromolecular composition of the feedstock was assessed by an external laboratory: lignin, cellulose, and carbohydrate content were measured using their internal

methodology (POM 017 Rev. 0 2011); additionally, proteins and lipids were assessed by ISTISAN 1996/34 pag.13 and CNR IRSA Met 21 Q 64 vol 3 1998, respectively.

The concentration of VFAs, including acetic, propionic, butyric, iso-butyric, valeric, isovaleric, and caproic acids, was measured using a gas chromatograph (7890B, Agilent Technology, Santa Clara, CA, USA) with hydrogen as the gas carrier, equipped with a CPFFAP column (0.25 mm/0.5 mm/30 m) and with a flame ionization detector (250 °C). Further details are reported in Baldi et al. [20].

To monitor process stability on the biogas samples, the concentrations of H_2, CH_4, CO_2, nitrogen (N), oxygen (O_2) and hydrogen sulphide (H_2S) were analyzed using a gas chromatograph (3000 Micro GC, INFICON, Bad Ragaz, SG, Switzerland) equipped with a thermal conductivity detector. CO_2 and H_2S passed through a PLOTQ column (10 mm/320 mm/8 m) using helium as the gas carrier at a temperature of 55 °C. The other gases passed through a Molsieve column (30 mm/320 mm/10 m) using argon as the gas carrier at a temperature of 50 °C [28].

2.5. Process Performance

The performance of the overall process was assessed by determining the concentration and composition of VFAs, biogas productivity and composition (CH_4 and CO_2), volatile solids reduction efficiency (REVS), and process stability. Below, each parameter used to monitor the process performance is defined. In addition, the optimal operating range is provided, if available.

VFA concentration and composition were evaluated as described in Section 2.4. Biogas productivity was assessed, including (i) daily biogas production as NLbiogas/d, which is evaluated using a volumetric counter, as described in Section 2.1, and converted from ambient into normal conditions of pressure and temperature (273.15 K and 1 atm, respectively) using the data from the sensors of atmospheric pressure and ambient temperature (Section 2.1); (ii) SGP as NLbiogas/kgVS, which is calculated by dividing the daily biogas production by the daily mass of VS fed to the reactor; (iii) specific methane production (SMP) as NLCH4/kgVS, which was evaluated by multiplying the SGP by daily average CH_4 concentration (%), and (iv) the biogas production rate (GPR) as NLbiogas/(L d), which is calculated by dividing daily biogas production (NLbiogas) by the reactor working volume (L). In addition, REVS (%) was calculated to evaluate the efficiency of the process to convert the inlet mass of VS in biogas, as follows, using Equation (3):

$$REVS = (VSin - VSout)/VSin \tag{3}$$

where VSin (%) is the VS content of inlet substrate, and VSout (%) is the total VS content of the outlet digestate.

Finally, process stability was monitored during the overall experimental tests in terms of pH, IA/PA ratio, FA, and TAN concentration. In detail, to ensure a stable dry AD process, these parameters should stay in the following ranges: pH = 6.5–8.2 [29], IA/PA $\leq$ 0.4 [9,26], FA < 600–800 mg/L [9], TAN = 1500–3000 mg/L [9].

2.6. Microbial Community Analysis

Bacterial ecology characterization is derived from the digestate sample, which showed the maximum VFA concentration.

The total DNA from the sludge coming from five different sections of the reactor (Figure 1) was extracted using the FastPrep 24™ homogenizer and the FAST DNA Spin Kit for soil (MP Biomedicals, Irvine, CA, USA), starting from 500 mg of the sample, according to manufacturer's protocol. Quantity of DNA was measured using the Qubit 3.0 fluorometer (ThermoFisher Scientific, Waltham, MA, USA). DNA purity and quality were determined spectrophotometrically (Biotek Powerwave Xs Microplate Spectrophotometer, Agilent Technology, Santa Clara, CA, USA) by measuring absorbance at 260/280 and 260/230 nm. A total of 200 ng of DNA was used to produce paired-end libraries and for sequencing the V4–V5 hypervariable regions of the bacterial 16S rRNA gene by using as primers

the 515F forward primer (5′-GTGCCAGCMGCCG CGGTAA-3′) and the 907R reverse primer (5′-CCGTCAATTCCTTTGAGTTT-3′). The libraries for Illumina sequencing were prepared using the NEBNext Ultra DNA Library Prep Kit, following the manufacturer's recommendations, and index codes were added. The library was sequenced on an Illumina platform by Novogene (Novogene Company Limited Rm.19C, Lockhart Ctr., 301–307, Lockhart Rd. Wan Chai, Hong Kong), and 250 bp paired-end reads were generated.

Data Analysis

Paired-end reads were demultiplexed and trimmed by the Cutadapt plugin for Qiime2. Forward and reverse reads were assembled, quality filtered, chimera filtered, and assigned to amplicon sequence variants (ASVs) following the Qiime2 v.2021.2 standard pipeline [30]. ASV clustering was performed using the DADA2 workflow implemented in Qiime2, with two classifiers trained on the V4–V5 hypervariable region extracted from the Silva 138 99% 16S sequences database. To allow comparison between different samples, ASV abundances per sample data were normalized by rarefaction to the same number of ASVs (43048 per sample). Subsequent analyses of α-diversity indexes (Chao1, Hill-Shannon, and Hill-Simpson diversity indexes, and rarefaction curves of observed species), β-diversity by principal coordinate analysis (PCoA) based on UniFrac distance, and other related statistical tests were performed in R 4.1.1 using Phyloseq, Vegan, and Pheatmap packages (versions 1.37.0, 2.5–7 and 1.0.12, respectively). Parametric statistics (Kruskal–Wallis test and related post-hoc tests) on chemical data were performed by ggpubr version 0.4.0.999. The functional metagenomic prediction for the bacterial community was inferred using PICRUSt2 v. 2.4.1 for unstratified and stratified metagenome contributions based on EC numbers, the MetaCyc pathway, and EC. Contributions were filtered from the output data of PICRUSt2 v. 2.4.1 and processed by R v. 4.1.1. Graphical output was produced by the ggplot2 package v. 3.3.5 and Pheatmap v. 1.0.12.

3. Results

3.1. Substrate and Inoculum Characterization

The average characteristics of the substrate fed to the reactor during the overall experimental period were 34.04 ± 5.36%, 77.42 ± 5.59%, 5.2 ± 0.41%, and 20.73 ± 5.26% of TS, VS/TS, pH, and C/N (n = 103), respectively. The average macromolecular composition of the feedstock on VS content basis was 35.12 ± 7.53%, 14.69 ± 2.95%, 1.63 ± 0.46%, 17.84 ± 3.62%, and 17.19 ± 5.43% of carbohydrates, proteins, lipid, lignin, and cellulose, respectively. In addition, Table 1 reports the variation of the substrate in terms of macromolecules (e.g., carbohydrates, proteins, lipid, lignin, and cellulose) in each sampling campaign. Finally, the inoculum had a TS content of 20.02 ± 0.02%, with a volatile solids content of 73.86 ± 0.20% and a pH of 7.95 ± 0.36.

3.2. Process Performances

3.2.1. VFA Production

Regarding VFA production, Figure 2 illustrates the concentration of total VFAs in the five sections in each sampling campaign.

In general, VFA concentration showed a positive trend with decreasing HRT. Starting from the longest HRT of 22 days (S1), T1 obtained the lowest total VFA concentration, ranging from 219.44 mg/L (sez.4) to 343.2 mg/L (sez.1). T2 and T3 showed a similar concentration of total VFAs, along with an analogous trend. In detail, VFA concentration was a parabolic curve with the maximum in sez.3 and the minimum in sez.5. The maximum concentrations were 1270.2 and 1066.2 mg/L, while the minimum was 791.9 and 947.3 mg/L for T2 and T3, respectively. Finally, T4 and T5 showed a VFA concentration higher than the other scenarios. Regarding T4, the VFA concentration started from the maximum in sez.1 (3244.14 mg/L) and decreased to the minimum in sez.5 (2348 mg/L). In contrast, for T5, the VFA concentration showed a parabolic trend. In the latter case, the parabola was asymmetrical, starting from 3106 mg/L (sez.1), then achieving the maximum

of 4421.8 mg/L in sez.4, and finally decreasing to 4186 mg/L (sez.5). Considering that T5 obtained the highest VFA concentration, as stated in Section 2.3, microbial ecology was investigated on this sample.
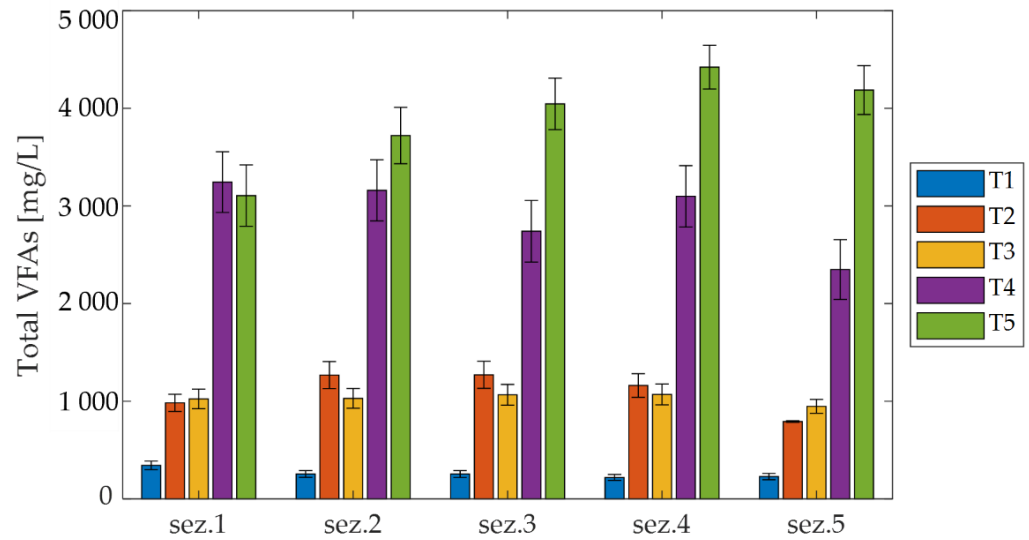

Figure 2. Total VFA concentration at sections sez.1–sez.5 in each sampling campaign.

Figure 3 illustrates the VFA spectrum in each sampling campaign and section. Acetic, propionic, butyric, and iso-valeric acids resulted in a share above 8% of total VFAs in at least one sampling campaign.
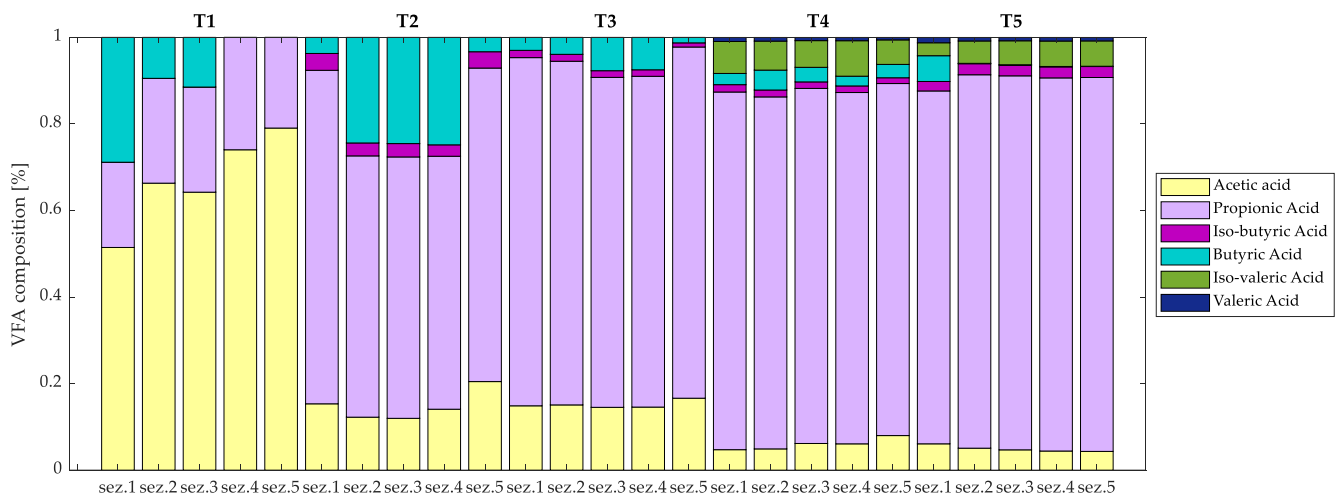

Figure 3. Composition of total VFAs at sections sez.1-sez.5 in each sampling campaign.

For the first sampling campaign, the spectrum of VFAs was a mix of acetic, propionic, and butyric acid. Acetate accounted for 51.5%, 66.3%, 64.2%, 74% and 79.1% in sez.1, sez.2, sez.3, sez.4, and sez.5, respectively. Propionic acid oscillated from 19.7% (sez.1) to 26% (sez.4) of total VFAs, while butyric acid decreased from sez.1 (28.8%) to sez.3 (11.5%) and was not detected in sez.4 and sez.5. When HRT increased, the share of propionate increased since T5 accounted for 81.6–86.4% of total VFAs. Going into more detail, T2 had propionic, butyric, and acetic acids as the main VFAs, while iso-butyric was below 4% of total VFAs. For this sampling campaign, propionic showed the greatest share in sez.1 (77.1%) and sez.5 (72.5%). In the other sections, propionic acid was slightly lower, accounting for 60.4%, 60.4%, and 58.5% in sez.2, sez.3, and sez.4, respectively, but the share of butyric acid increased to around 24.5%. In the third sampling campaign, T3, propionic acid still dominated among the other acids: acetic acid was the second intermediate product

(14.5–16.6%); butyrate dropped (7.7–1.2%) as well as iso-butyrate (1.6–1.1%). However, differently from T2, the share of propionic acid was almost constant among the sampling sections (80.5%, 79.4%, 76.3%, 76.4%, and 81.2% in sez.1, sez.2, sez.3, sez.4, and sez.5, respectively). In the sample of T4, propionic acid was around 81.2–82.7%, the share of acetic acid decreased to 4.7–8%, and butyric and iso-butyric acid did not change, while iso-valeric acid was detected, accounting for 7.4%, 6.7%, 6.2%, 8.2%, and 5.7% in sez.1, sez.2, sez.3, sez.4, and sez.5, respectively. Finally, in the last sample (T5), propionic increased its share, ranging from 86.4% to 81.6%; acetate decreased with respect to T4 as well as butyric acid and iso-valeric acid, which were below the 6% of total VFAs. In detail, at the end of S3, the acetate concentration was three times higher than propionate.

3.2.2. Biogas Production

Going to biogas productivity, Figure 4 shows the daily biogas production during the experimental period. Focusing on S1, biogas production increased to the maximum of 89.4 NLbiogas and then decreased to the minimum of 47.2 NLbiogas. At the same time, FA increased above the inhibition limit for AD of 350 mg/L, reaching 1350 mg/L (data not shown). During S2, the FA concentration decreased to 779 mg/L and biogas production slightly increased to 66.6 ± 15.16 NLbiogas on average. A similar trend was also highlighted for the SGP and SMP (data not shown). During S3, FA concentration decreased, and biogas production increased and stabilized at around 138 ± 11.7 NLbiogas (days 130–150).
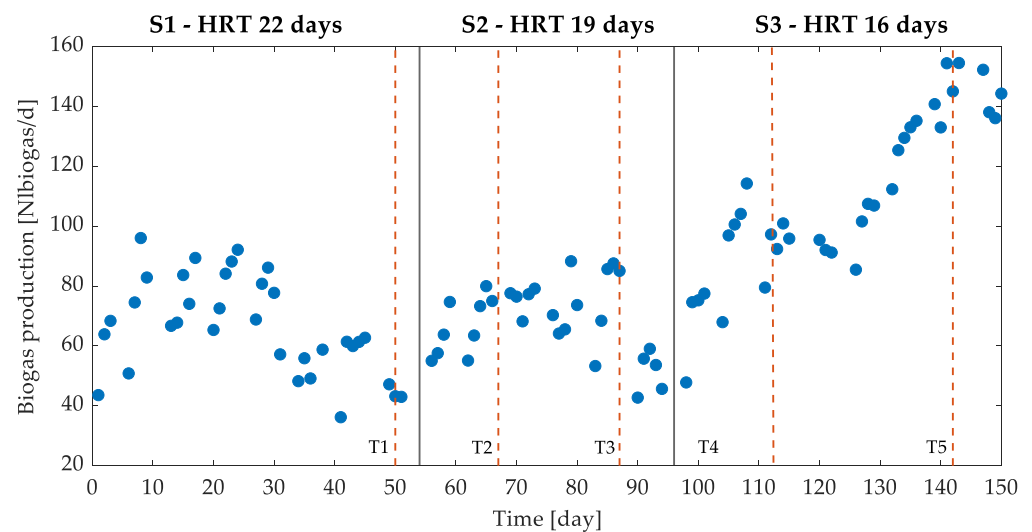
Figure 4. Biogas production during the experimental period. Continuous lines indicate different scenarios, while dashed lines indicate digestate sampling campaigns. Sample T5 was analyzed for bacterial ecology.

Since VFA characterization was performed on digestate samples withdrawn from the PFR during five different sampling campaigns, the following table summarizes the process performances in terms of biogas productivity on each sampling date. To deeply explain the results, a mass balance on VS was performed. Then, the results were compared to those calculated by Equation (1). In detail, the percentage change resulted in −1.65%, 8.63%, and −2.68% change for S1, S2, and S3, respectively, thus being in line with the experimental data. In addition, considering a mass balance on lignin, the results show that lignin accumulates inside the digester as HRT decreases, reaching a negative reduction efficiency of −47.05% for S3. Thus, a share of carbon leaves the PFR reactor without being transformed into biogas.

3.3. Bacterial Community Analysis

Bacterial community analysis was performed firstly by evaluating the global effects on the number of different taxa and their relative abundance distribution across each section of the AD: these factors contribute to community diversity, which is expressed by richness (e.g., Chao 1) and evenness (e.g., Hill–Simpson and Hill–Shannon) indexes comprised in the α-diversity evaluation reported in Figure 4.

The results obtained a figure that did not evidence a neat effect of community speciation or selection processes along the reactor profile: the Chao1 index (panel A), an estimator of the number of different taxa, reports a value around 200, which does not significantly vary along the sections.

Both Hill–Simpson and Hill–Shannon are equidistributional indexes: the higher they are, the more similar the number of counts for each taxon. The values reported in panel B and panel C of Figure 4 are very low and do not evidence a significant variation except for an increase for the Hill–Simpson index (panel C) in sez.2 and sez.4, with reference to sez1. Panel D reports the rarefaction curves, which allow us to evaluate if the sequencing depth was enough to catch a representative picture of the microbial community: the faster the curve reaches a plateau, the more the sequencing depth is redundant; additionally, rare species are correctly depicted.

β-diversity analysis is based on a hierarchical classification (by principal component analysis) that allows the evaluation of similarity/dissimilarity between microbial communities: the chosen distance (weighted UniFrac) takes into consideration both phylogenetic similarities between each contributing taxa and their abundance.

Figure 5 provides evidence that biological replicates constituting sez.1 and sez.5 clusters are well defined, while sez.2 replicates show less inter-sample homogeneity (i.e., a bigger spread of data points in comparison to sez.1 and sez.5); sez.3 and sez.4 data points are mixed in a single cluster.

The last part of microbial community analysis focuses on differential abundance analysis of the most abundant (and thus the most influential) taxa across the AD section. This analysis can be performed at each taxonomical level: in this article, we focus on class (Figure 6) and genus (Figure 7) abundances.

As reported in Figure 7, three classes of bacterial species were higher than 1%: *undefined_Thermotogae* (72.72%), *Clostridia* (14.56%), and *Bacteroidia* (9.92%). In detail, *undefined_Thermotogae* had the maximum relative abundances in sez.1 and sez.5, while on the opposite side, *Clostridia* were more abundant in the central sections (sez.2, sez.3, sez.4). Differently, *Bacteroidia* had the lowest relative abundance in sez.1.

Since *Clostridia* are the second most represented class inside our reactor, major effort was taken in order to refine the taxonomic assignment of the members of this class. Among the 20 most abundant taxa in our reactor, 6 belong to *Clostridia*: the 8th, 14th, and 16th most abundant taxa are classified at the genus level as *Caldicoprobacter* sp. (0.55%), *Syntrophaceticus* sp. (0.09%), and *Syntrophomonas* sp. (0.06%). The representative sequences of the 2nd, 5th, and 6th most abundant taxa (still belonging to *Clostridia,* but not more precisely identified), corresponding, respectively, to 8.18%, 3.10%, and 0.71% of the total when manually submitted to a BLASTn alignment, resulting in uncultured microorganisms (data not shown).

At the genus level (Figure 8), the class *Undefined_Thermotogae* was assigned to the *Defluviitoga* sp. *Defluviitoga* sp. was the most abundant bacterial genus (72.72% on average), followed by *Unclassified* bacterial species (12.73%), *unidentified_Lentimicrobiaceae* (5.52%), and *Proteiniphilum* (4.36%). Sez.1 and sez.5 showed the highest relative abundance, while *Unclassified* bacterial species prevailed in the other sections. *Unidentified_Lentimicrobiaceae* and *Proteiniphilum* sp. had a lower relative abundance in sez.1 than in the other sections.
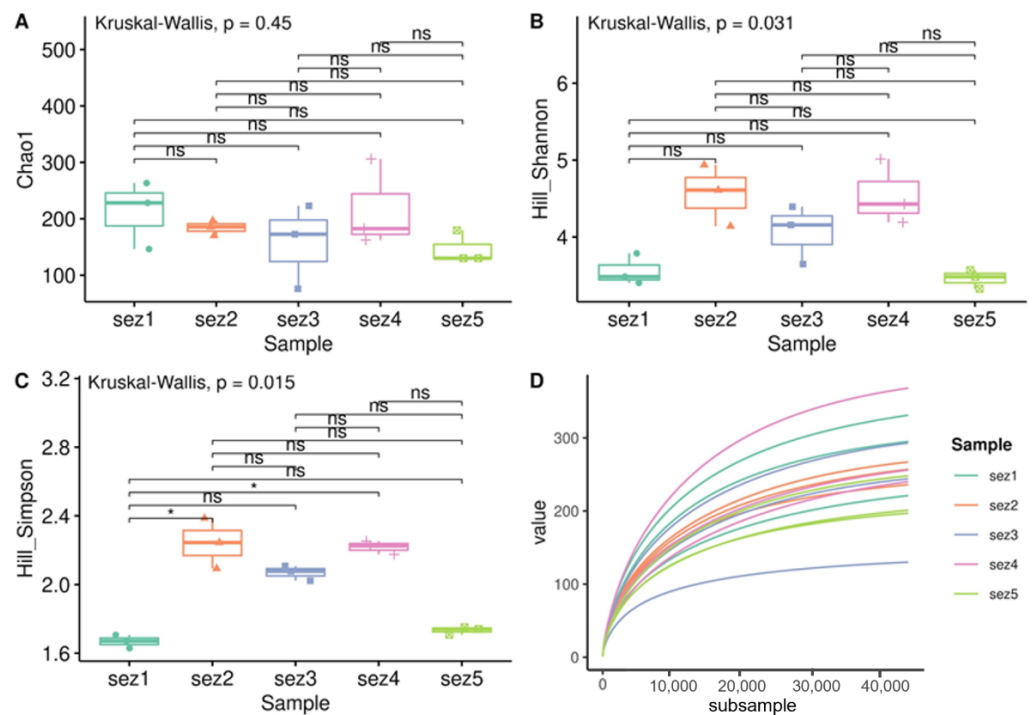
Figure 5. Bacterial community analysis: (**A**) α-diversity represents the Chao1 index; (**B**) Hill–Shannon; (**C**) Hill–Simpson index, each calculated after rarefaction to a coverage of 99.5%, and (**D**) rarefaction curves of observed species of bacterial community composition. Box and whiskers represent the minimum, 1st quartile, median, 3rd quartile, and maximum of each group. The reported *p*-value is calculated by the Kruskal–Wallis test (α = 0.05); the post-hoc statistical test is based on the Dunn test, with Benjamini–Hochberg corrections for multiple comparisons: Notations for the *p*-value is the following: ns for $p > 0.05$; * for $p \leq 0.05$.
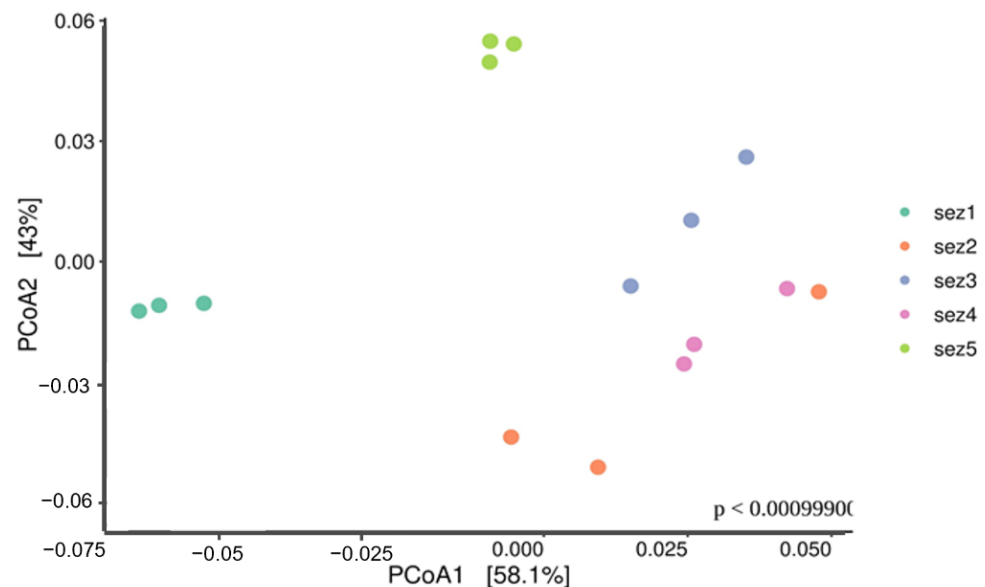
Figure 6. Principal component analysis (PCoA) based on weighted UniFrac distances for each sample replicate. Colors indicate the sampling section of the plug-flow reactor for each data point. The percentage reported on axes represents the amount of total variance depicted by each of them. The *p*-value was calculated by the ADONIS function (Vegan R package v 2.5–7) between weighted UniFrac distances and sample groups using the Bray–Curtis method with 1000 repetitions.
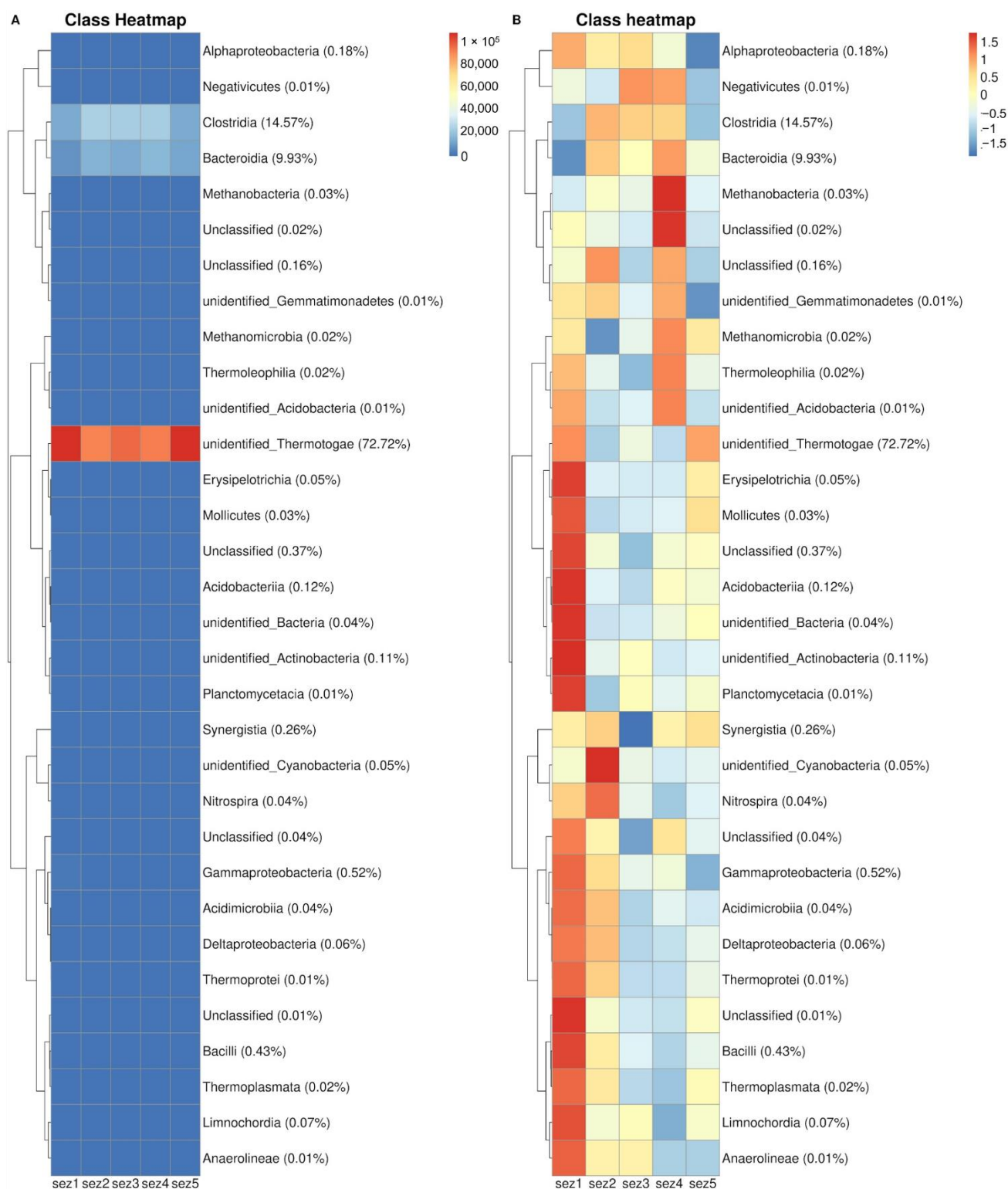
Figure 7. Taxonomic heatmaps at the class level. Taxonomic heatmaps showing the most abundant ASVs per section: (**A**) absolute counts and (**B**) autoscaled counts, aggregated at the class level. Percentages reported near the ASV names represent the relative abundance of the sum of ASV counts per sample against the total sum: a cut-off value of 0.005% was chosen. Hierarchical clustering was performed on rows by Pearson correlation, based on Euclidean distance. In order to evidence variation, the color scheme of panel B, representing row-wise Z-scores of ASV counts per sample, was chosen. For this color scheme, a Z value of 0 matches the reported percentage near the ASV names.
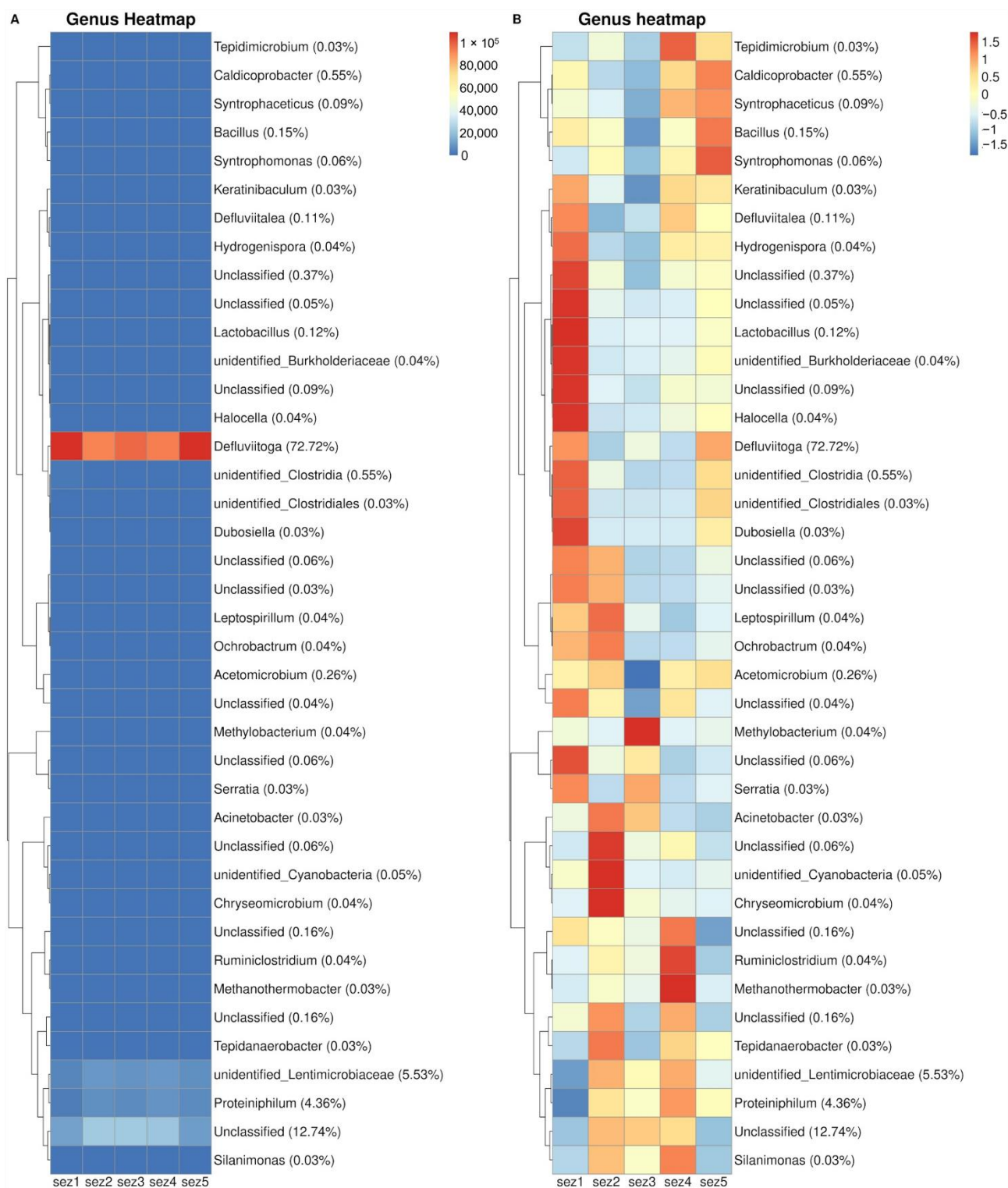
Figure 8. Taxonomic heatmaps at the genus level. Taxonomic heatmaps showing the most abundant ASVs per section: (**A**) absolute counts and (**B**) autoscaled counts, aggregated at the genus level. Percentages reported near the ASV names represent the relative abundance of the sum of ASV counts per sample against the total sum: a cut-off value of 0.005% was chosen. Hierarchical clustering was performed on rows by Pearson correlation, based on Euclidean distance. In order to evidence variation, the color scheme of panel B, representing row-wise Z-scores of ASV counts per sample, was chosen. For this color scheme, a Z value of 0 matches the reported percentage near the ASV names.

Functional Analysis

Figure 9 shows the contribution to hydrolytic enzyme families and hydrogen-related enzymes in the five sampling sections. During the AD process, three main groups of enzymes were found to be involved in the hydrolysis of the organic matter: esterases, glycosidases, and peptidases [31]. The contributions to the enzymes are implied in hydrogen consumption (ferredoxin hydrogenase EC: EC:1.12.7.2) and production (nitrogenase EC:1.18.6.1), and the former, due to the hydrogen cycling capability of some acetogens such as *Acetobacterium woodi* [32], as inferred by PICRUSt2. Both retrieved contributions show a minimum in sez.3. The major contributions to ferredoxin hydrogenase are, at the class level (Figure A7), from *Synergistia* (73.43%), followed by *Clostridia* (12.21%). At the genus level (Figure A8), the major contributors were *Acetomicrobium* sp. (73.43%), the sole representative of the class *Synergistia*, and *Syntrophomonas* sp. (5.18%), which belongs to class *Clostridia*. The absolute heatmaps revealed that *Synergistia* were abundant in all the sampling sections except for sez.3. *Clostridia* were more abundant in sez.5 than in the other sections. Nitrogenase activity is performed at the class level mainly by *Clostridia* (71%) and at the genus level by an unclassified genus of the *Rumnicoccaceae* family (38.96%), *unclassified_Burkholdeliaceae* (15.32%), *Ruminclostridium* sp. (10.60%), *Syntrophaceticus* sp. (6.24%), and *Syntrophomonas* sp. (3.95%) (Figure A9). The global trend of nitrogenase is bimodal: the first maximum in sez.1 was mainly due to *unclassified_Burkholdeliaceae*, followed by a minimum in sez.3 and a plateau in sez.4 and sez.5, where the unclassified genus belonging to *Rumnicoccaceae*, *Ruminclostridium*, *Syntrophaceticus*, and *Syntrophomonas* sps. are the main contributors.

(**a**)   (**b**)
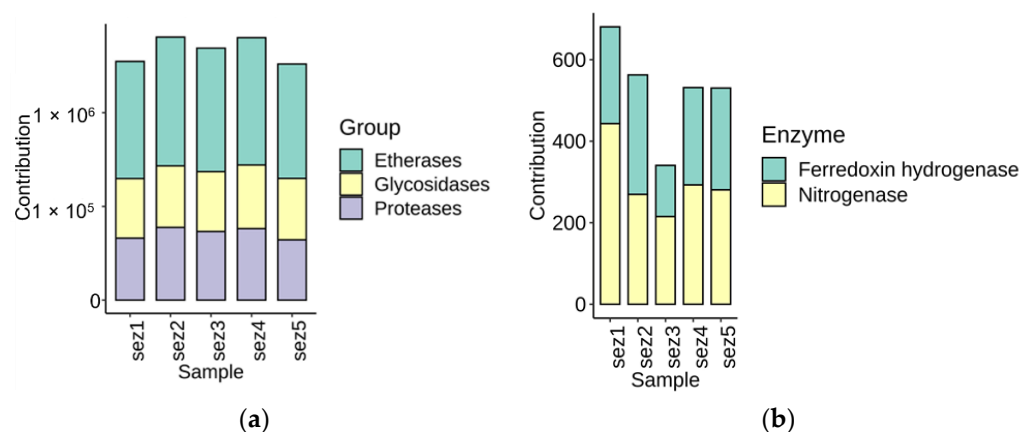
Figure 9. Contributions to hydrolytic enzyme families and hydrogen-related enzymes. (**a**) Hydrolytic enzymes are reported as a sum of esterases (EC:3.1.-), glycosidases (EC:3.2.-), and proteases (EC:3.4.-) for each sampling section; (**b**) hydrogen-related enzymes: ferredoxin hydrogenase and nitrogenase contributions; the numbers reported are the mean of the sum of contributions per taxa in each AD section, calculated by PICRUSt2.

Figure 10 illustrates the pathways involved in VFA production. Details on the predictive functional metagenomic analysis are reported in Appendix A. All the pathways listed in MetaCyc that lead to VFA production were queried after filtering the PICRUSt2 results for a coverage of 60%. The list of queried pathways is provided in Appendix B. However, only P163-PWY, PWY-5100, and P108-PWY were found: L-lysine fermentation to acetate and butanoate, pyruvate fermentation to acetate, and lactate II and pyruvate fermentation to propanoate I. Starting from L-lysine fermentation to acetate and butanoate, the functional heatmap at the class level (Figure A1) showed that *unidentified_Thermotogae* were the only bacteria responsible for this metabolic pathway accounting for 99.65% (with two relative maxima in sez.1 and sez.5). At the genus level, *unidentified_Thermotogae* were represented by *Defluviitoga* sp., the bacterial genus responsible for this pathway (Figure A2).
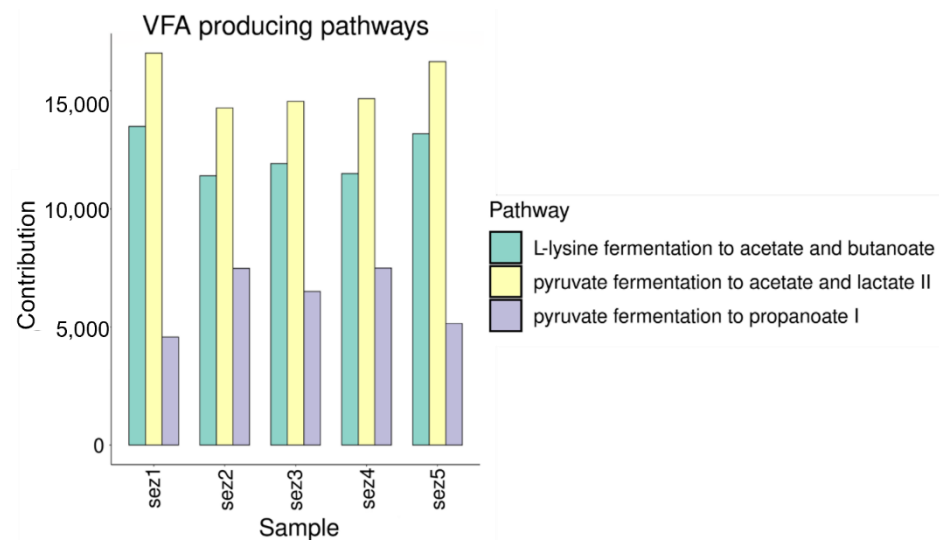
Figure 10. Contributions to pathways involved in VFA production. The numbers reported are the mean of the sum of contributions per taxa in each AD section, calculated by PICRUSt2.

With reference to pyruvate fermentation to propanoate I, the functional heatmap with absolute counts (Figure A3) shows that *Bacteroidia* and *Clostridia* were mostly involved in this metabolic pathway, accounting for 64.77% and 28.66%, respectively. Specifically, sez.4 and sez.2 reached the highest absolute abundance. At the genus level, the functional heatmap with absolute counts showed that *unidentified_Lentimicrobiaceae* (46.63%), *Proteiniphilum* sp. (17.9%), and *Unclassified* bacterial species (28.66%) were dominant to the other bacteria (Figure A4). Focusing on the relative heatmap, all the bacteria involved in this pathway increased their relative contribution in the central area of the reactor (sez. 2, sez.3, sez.4).

Finally, pyruvate fermentation to acetate and lactate II revealed that at the class level, *unidentified_Thermotogae* were involved in this metabolic pathway, accounting for 83.37% on average (Figure A5). The *Bacteroidia* were the second most abundant class, with 6.21% (Figure A5). At the genus level, *Defluviitoga* sp., dominated with an average abundance of 83.73% (Figure A6).

4. Discussion

4.1. VFA and Biogas Production

The first goal of the study was to assess the performance of VFA production by dry thermophilic AD of OFMSW in a PFR. However, biogas (which is the main voluminous outlet stream of the process) and the performance of the process are evaluated towards further valorization in a biorefinery approach. The overall VFA and biogas productivity are discussed by comparing the results with those reported in the state-of-the-art facilities.

Starting from VFA production, the fermentation of food waste is generally associated with a high concentration of total VFAs and a variable final spectrum of VFAs, depending on the macromolecular composition of the feedstock and operating parameters such as HRT, OLR, pH, temperature, and the recirculation ratio. Focusing on VFA concentration, the process reached a maximum VFA concentration of 4421.8 mg/L, which is lower than the typical range of 15–30 g/L reported in the literature during food waste fermentation [5]. This is because the process is not solely optimized for VFA production since the aim is to produce both VFAs and biogas. VFA concentration is inversely correlated with the HRT. This result could be explained by considering that for low HRT after hydrolysis and acidogenesis, VFAs can only be partially further converted in CH_4 since the retention time is too low for methanogenic archaea [33]. On the contrary, when retention time increases, the substrate is hydrolyzed and then monomers are converted into VFAs, which can be further used to produce CH_4. In this study, the combined effect of shorter HRT and higher

OLR positively affected VFA concentration since the higher OLRs, the higher the hydrolysis and acidogesis rates [5,33]. Furthermore, this fact is consistent with the percentage of VFAs calculated in relation to sCOD as VFAs appear to increase as HRT decreases (the percentage of VFAs/sCOD equals T1: 1.4%, T2: 3.1%, T3: 4.3%, T4: 12.1%, and T5: 22.7%, respectively).

The VFA concentration along the digester displayed a parabolic trend for each sample except for T4. A possible explanation of this result is the functioning of PFR, where the substrate ideally moves horizontally from the inlet to the outlet. This characteristic might promote hydrolysis near the inlet, then acidogenesis and acetogenesis in the central zone, and, finally, methanogenesis near the outlet. This attitude was also confirmed by the results of bacterial characterization, which showed a prevalence of *Defluviitogae* sp. in sez.1 and sez.5. Instead, *Bacteroidia* and *Clostridia,* which are acidogenic bacteria [17,34], prevailed in sez.2, sez.3, and sez.4. In fact, *Defluviitogae* sp. are hydrolytic bacteria [35] associated with thermophilic dry AD of OFMSW at high OLRs [36,37] as described in detail in Section 4.2. To understand these outcomes, it is also necessary to consider the inoculation of inlet feedstock with the partially recirculated outlet digestate. From the results, feedstock inoculation seems to promote the initial hydrolysis and acidogenesis of organic matter since the VFA concentration is higher at the inlet (sez.1) than at the outlet (sez.5). However, this effect is particularly clear when HRT is long, for example, for samples T2 and T3. Instead, the effects of a short HRT dominate at recirculation. In fact, sample T5 has a concentration of VFAs higher at the outlet (sez.5) than at the inlet (sez.1). This explanation might justify (even if not completely) the similar behavior and the bacterial composition of sez.1 and sez.5. Nevertheless, the PCoA (Figure 5) indicates a different microbial composition from sez.1 and sez.5 since the clusters of each section are significantly distant. A similar result was obtained in a recent study that analyzed the effects of digestate recirculation on microbial composition during dry AD of corn straw [19]. Specifically, the authors found that by increasing the recirculation ratio to 60%, the inlet sample had a distinct bacterial composition compared to the outlet sample.

In relation to VFA composition, propionate dominated in the other short-chain acids (i.e., acetic, butyric acid, iso-butyric, valeric and iso-valeric acids) that are produced by food waste fermentation [5]. In fact, OFMSW generally produced a variegate VFA spectrum, thus resulting in a mixed-type metabolic pathway [34,38]. Within the literature, several studies investigated the causes leading to different total VFA compositions, but the results were not always in agreement since the final products strictly depend on both feedstock composition and operating parameters. For example, during food waste fermentation, butyric acid accounted for 69% of total VFAs in thermophilic and acid conditions, while acetate dominated at alkaline pH [15]. In contrast, the production of propionic acid is commonly associated with protein-rich substrates [5] as it is the OFMSW used in this study. In fact, protein content ranged between 10.04–16.98% VS, which is a typical value for OFMSW [39]. In addition, the pH of the process was close to alkaline conditions (i.e., 8.1–8.37), which is associated with propionate production [40]. In addition, a recent study found that reducing HRT from 40 to 20 days led to an increase of propionate concentration from 1010 to 5820 g/L [41]. Analogously, in this study, when HRT decreased from 22 to 16 days, propionate increased from 20% to 86% of total VFAs. Iso-butyric, valeric, and iso-valeric acids are the secondary fermentation products of this process. Generally, these compounds are less present than acetate, propionic, and butyric acids during OFMSW fermentation. In fact, iso-butyric acid was always below 4% of total VFAs; in contrast, iso-valerate reached 8.2% of total VFAs. Despite the fact that the relative percentage is low, the finding of such a share of iso-valeric acid was unexpected. In fact, iso-valerate is generally found during alkaline fermentation of sewage sludges (SS) [42] by reduction of pyruvate [7]. Since iso-valerate production derives from proteins, the high content of the latter in the feedstock is at the origin of the result obtained. Recirculation of digestate seems not to affect VFA composition except for T2. In the latter case, Figure 3 clearly shows that sez.1 and sez.5 have an analogous spectrum of VFAs. However, it is clear that the

composition of final products seems to be more strongly related to HRT than to digestate recirculation.

With regard to biogas production, the performances of the process studied here were slightly lower than those commonly reported in the literature for dry AD of OFMSW [8]. Focusing on SMP, typical values range between 230–490 $NLCH_4/kgVS$ [8], but we obtained 103.9–247.3 $NLCH_4/kgVS$. Probably this effect has a twofold cause. Firstly, the OFMSW characterization revealed a lignin content of $17.84 \pm 3.62\%$ for volatile solids, which is far higher than the $9.7 \pm 5.3\%$ (on a VS basis) reported within the literature as the average value for OFMSW [39]. More in detail, lignin is a recalcitrant compound for AD [43], and it is an indicator of low biogas production [39]. Secondly, the results reported in Table 2 suggest that the process suffered from ammonia inhibition. In detail, inhibitory concentration ranges between 1500–3000 and 600–800 mg/L for TAN and FA, respectively [8,9], and, in this study, FA concentration ranged from 1132 to 393 mg/L. Dry AD is more prone than wet AD to ammonia inhibition, especially for protein-rich substrate, as it is OFMSW [9]. Both TAN and FA, which originate from the hydrolyzation of proteins, inhibit bacterial populations through several mechanisms [44]. However, FA was highlighted as the main cause of inhibition since it is able to cross the bacterial membrane [44]. To alleviate FA inhibition, a promising strategy is altering the feedstock to increase the C/N ratio [12]. As a consequence, the C/N ratio was increased from 18 to 32. When C/N was 32, the FA concentration decreased, while biogas production and GPR increased. Concerning process stability, during the overall experimental period, the IA/PA ratio oscillated between 0.49 and 0.73, resulting in a higher-than-optimal value of 0.3 for a stable AD process [29]. However, the reactor never failed. This was because the IA/PA ratio was found to be not reliable for monitoring AD stability when FA inhibition occurs [21].

Table 2. Process performance in each digestate sampling campaign.

Parameter	T1	T2	T3	T4	T5
pH [-]	8.37 ± 0.41	8.33 ± 0.41	8.25 ± 0.41	8.24 ± 0.41	8.1 ± 0.4
IA/PA [-]	0.49 ± 0.04	0.59 ± 0.05	0.59 ± 0.05	0.52 ± 0.05	0.57 ± 0.05
TAN [mg/L]	2177.7 ± 108.88	3356.1 ± 167.8	2877.7 ± 143.88	1870.5 ± 93.52	1081.1 ± 54.05
FA [mg/L]	1034.8 ± 51.74	1132.3 ± 56.61	1092.7 ± 54.63	751.3 ± 37.56	393.09 ± 19.65
Biogas [NLbiogas/d]	43.21 ± 2.16	75.02 ± 3.75	85.08 ± 4.25	92.38 ± 4.61	145.03 ± 7.25
SGP [NLbiogas/kgVS]	182.2 ± 9.11	339.83 ± 16.99	429.99 ± 21.49	326.02 ± 16.3	364.04 ± 18.2
SMP [$NLCH_4$/kgVS]	103.87 ± 5.19	198.69 ± 9.93	247.27 ± 12.36	165.08 ± 8.25	237.8 ± 11.89
GPR [NLbiogas/(lr d)]	1.56 ± 0.07	2.82 ± 0.14	3.12 ± 0.15	3.24 ± 0.16	5.11 ± 0.25
VSout [%]	69.78 ± 0.13	67.3 ± 0.13	63.96 ± 0.12	62.06 ± 0.12	62.68 ± 0.12
REVS [%]	52.91 ± 0.21	42.33 ± 0.16	40.09 ± 0.16	45.38 ± 0.18	52.1 ± 0.2
CH_4 [%]	56.85 ± 2.53	58.47 ± 2.72	57.64 ± 2.62	50.63 ± 1.84	65.32 ± 3.61
CO_2 [%]	43.15 ± 1.16	41.53 ± 1.03	42.36 ± 1.09	49.37 ± 1.72	34.68 ± 0.55

To sum up, in a biorefinery approach, the optimal results were achieved in terms of both VFA production and biogas production during S3. In detail, the concentration of VFA reached 4421.8 mg/L at sez.4, while daily biogas production was 145.03 ± 7.25 NLbiogas/d. This point could be used to withdraw digestate for a further application of the VFA-rich digestate. However, the retrieval of digestate could reduce biogas production, and, for this reason, further investigation should be conducted, specifically performing a mass balance on the system and, consequently, optimizing the process to produce VFAs or biogas.

4.2. Microbial Analysis

In relation to microbial ecology, the discussion focuses on the findings related to sample T5. This sample was characterized for this aspect since it showed the maximum VFA concentration among the other samples; FA and the TAN concentration were below the inhibition threshold for dry AD, and the process achieved the highest biogas production of the overall experimental period.

α-Diversity suggests that the analyzed bacterial community is quite low in comparison to other bacterial communities in various anaerobic digestion processes [45–47]. The evenness recovered in the PFR is one order of magnitude lower than the above reported microbial communities. The time course of the Hill–Simpson index, observed here, suggests that the contribution of not-dominant bacterial is increased in the central sections of the reactor.

The differential abundance gives evidence that the reactor is dominated by a limited number of diverse taxa, thus suggesting that PFR operating conditions, mainly due to the thermophilic temperature and a hardly hydrolyzable feed (i.e., lignin content of the feedstock 13.99–24.84%VS), limited the bacterial biodiversity in the reactor. Similar results were previously highlighted during the anaerobic digestion of vegetable wastes for thermophilic and high VS feed [48].

Due to the taxa distribution that we observed along the reactor profile, it is reasonable to suggest that two different hydrolytic phases of complex polysaccharides take place in sez.1 and sez.5. The two hydrolytic sections are separated by a partial hydrolytic process of the proteic fraction and lignocellulosic material that are performed in sez.2, sez.3, and sez4. In detail, *Defluviitoga* sp. is the main bacterial genus responsible for the hydrolytic activity. Phylum *Thermotogae*, which is dominant among the other bacteria, is generally associated with the thermophilic AD of food waste at high OLRs [36,49]. The phylum is, here, totally represented by *Defluviitoga* sp., described as playing an important role in organic matter degradation [35]. Since the taxonomically most similar bacteria, whose genome was sequenced and annotated, is the *Defluviitoga tunisiensis* L3, described as an anaerobic bacterium that presents complete pathways for the hydrolysis and metabolization of complex polysaccharides such as cellulose, chitin, and xylans, up to acetate, hydrogen and carbon dioxide [50], it is reasonable to suggest that the two observed maxima in *Defluviitoga* sp. representativeness indicate two different hydrolytic phases of complex polysaccharides occurring in two different sections of the reactor: sez.1 and sez.5. Their activity in the first section is reasonably associated with the increase in the representativeness of *Bacteroidia* and *Clostridia* in sez.2, sez.3, and sez.4, more precisely, for *Bacterioidia*, in *Lentimicrobiaceae* and *Proteiniphilum* sp. abundances. The *Lentimicrobium saccharophilum* are able to grow in a narrow range of carbohydrates under anaerobic conditions [51]. In this context, the carbohydrates transformed by *Lentimicrobiaceae* are released by *Defluviitoga* sp. hydrolytic activity in sez.1. The major fermentative end products by *Lentimicrobium* sp. are acetate, malate, propionate, formate, and hydrogen. *Proteiniphilum* sp. has its own relative maximum abundance in sez.4. It is described as a strictly anaerobic proteolytic bacterium. Two strains are described in the literature in relation to AD: *P. acetatigenes*, mesophilic, isolated in brewery anaerobic digesters, uses pyruvate, glycine and l-arginine as carbon and energy sources and no carbohydrates [52]; *P. saccharofermentans* sp., described as facultatively anaerobic and mesophilic, ferments proteins and complex sugars to CO_2, H_2, acetate, formate, propionate, and iso-valerate as end-products [53]. The temperature of PFR and the section in which *Proteiniphilum* sp. reaches its maximum abundance suggest that the proteolytic process takes place in the central sections of PFR. This is in line with the evidence of VFA-increased production (especially propanoate) in the central sections due to protein fermentation processes that are carried out after simple carbohydrate fermentation [54].

In the PFR, the majority of taxa assigned to the *Clostridia* class is not better addressed at lower taxonomic levels, with the exception of *Caldicoprobacter, Syntrophomonas*, and *Syntrophaceticus* sp. The class is generally described as sporulating strictly anaerobic organisms, responsible for the fermentation of complex sugars into lactate, ethanol, and hydrogen [55] and lignocellulosic derivatives such as xylans [56]. The process might be responsible for the production of cellulose amounts that allow a second blooming of *Defluviitoga* sp. and the related hydrolytic activity of sez.5. The *Clostidria* global effect on fermentation might be similar to that of *Bacteroidia*, which showed an analog representativeness pattern in the PFR sections. There are many examples of members of the *Clostridia* slass that are capable of exploiting protein fermentation for growth [57–59]. For this class, taxonomic assignment

is not enough to infer their role in our PFR process. In fact, among the individuated genera belonging to *Clostridia* that increase their relative abundance in sez.4, we find *Caldicoprobacter* sp. The *Caldicoprobacter* sp. includes four isolated species, described in the literature, all thermophilic and neutrophilic and able to ferment complex sugars into lactate, ethanol, and hydrogen [55]; three of four species are able also to ferment lignocellulosic derivatives such as xylans.

The other two identified genera belonging to the *Clostridia* class, more precisely *Syntrophaceticus* sp. and *Syntrophomonas* sp., are implied in the acidogenesis and acetogenesis phases. In relation to *Syntrophaceticus* sp., one strain [60] is described in the literature: the strain *S. shinkii* was isolated in a mesophilic methanogenic digestor at high ammonium concentration, and it is a syntrophic growing bacterium, capable of utilizing ethanol, betaine, and lactate as carbon and electron sources. Due to a minor inhibition by ammonium and the VFA concentration, *Syntrophaceticus* sp. can effectively compete with acetoclastic methanogenic *Archaea* on acetate scavenging, driving biogas production toward hydrogen gas [61]. On the other hand, in relation to the *Syntrophomonas* sp., six cultured strains have been described [62]. All the *Synthromonas* strains are described as synergistic-growing anaerobic bacteria that can metabolize short-chain fatty acids produced during the acidogenesis phase [55]. The relative abundance of *Caldicoprobacter, Syntrophomonas,* and *Syntrophaceticus* sp. increases in the last two sections, corroborating that the second hydrolysis stage, suggested by *Defuviitoga* bimodal distribution, could be performed in consequence of partial lignin depolymerization and freed cellulose processing.

In relation to *Archaea, Thermoprotei, Thermoplasmata,* and *Anaerolinea* show a prevalence in sez.1, suggesting that these classes originate from the microbial community of the feed and are no further enriched by the fermentation processes performed along the PFR. *Methanobacteria* and *Methanomicrobia* have their relative maximum in sez.4 and sez.5, suggesting that the methane production process is mainly performed in the final stages of the PFR.

A more detailed analysis of the possible role of the bacteria retrieved can be performed by metabolic pathway inference on the basis of the nearest sequenced microorganisms, performed by PICRUSt2. Here, we focus on the pathways and enzymes characteristic of the three phases of the AD that can be carried out by bacteria: hydrolysis, acidogenesis, and acetogenesis.

Regarding the hydrolysis step, the total amount of hydrolytic enzymes shows a homogeneous distribution in all sections: the most evident changes are related to proteases, and these are mostly pronounced in the central sections (sez.2, sez.3, and sez.4), following the pattern of *Clostridia* and *Bacteroidia* abundances, confirming their involvement in the process.

Focusing on the trend of each metabolic pathway for VFA production and the associated contribution per taxa, *Bacteroidia* and *Clostridia* are highly correlated to the propanoate production trend per section. As already reported, both *Proteiniphilum* sp. and *Lentimicrobiaceae* families are involved in the fermentation of sugars and amino acids.

Among the enzymes implied in hydrogen production, which is performed during theacetogenesis phase, Nnitrogenase and ferredoxin hydrogenase were the most relevant. The nitrogenase enzyme is implied in nitrogen fixation into ammonia [63]. This reaction produces one equivalent of hydrogen per nitrogen fixed: this reaction is not reversible, being one certain source of hydrogen gas production. The nitrogen-fixing microbial community is favored at less acidic conditions than those found in the PFR [63]. Ferredoxin hydrogenase can actually catalyze electron transfers from reduced ferredoxin to a proton, or reversely, an electron from molecular hydrogen to an oxidized ferredoxin with fine tuning [64]. Ferredoxin hydrogenase is also present in hydrogenotrophic methanogenic *Archaea*, where it generally works towards the consumption of such a gas, with the notable exception of hydrogenogenic carboxydotrophic thermophilic *Archaea* [65]. Notably, among the existing species of *Acetomicrobium* sp., *A. hydrogeniformans* has the ability to produce molecular

hydrogen from simple sugar fermentation [55] and is dominant in the favored syntropic dry AD settings [37].

Both these enzymes evidence that microbiological activity toward hydrogen production (nitrogenase) and hydrogen production/consumption (ferredoxin hydrogenase) shows an arrest in the central section of AD, corroborating the hypothesis already suggested by the distribution profile of *Defluviitoga* sp.: two hydrolytic phases, followed by released sugars and amino acid fermentation to hydrogen and acetate, are performed through the reactor profile.

Even if the major contributions to ferredoxin hydrogenase are from *Acetomicrobium* and *Syntrophomonas,* suggesting that the bacterial contribution to hydrogen metabolism inside our PFR is toward hydrogen production, this gas contributes only to traces (70–90 residual ppm) of biogas composition at the end of the PFR. This suggests that hydrogenoclastic *Archaea,* such as the retrieved *Methanothermobacter,* have relevance in the methanogenic process.

5. Conclusions

This study improves the understanding of dry anaerobic digestion biorefineries. Specifically, dry thermophilic AD of OFMSW provides a good alternative to wet technologies in both the production of volatile fatty acids (VFAs), as chemicals building blocks and the production of biogas for energy recovery. In addition, the effects of the HRT on the process were evaluated. The concentration of VFA was inversely correlated with hydraulic retention time, reaching the maximum of 4421.8 mg/L when HRT was minimum, namely, 16 days. Inside the PFR, the concentration of VFAs was a parabolic curve with the maximum in the central zone but nearer to the outlet. As a consequence, this section could be used to withdraw digestate to further valorize this VFA-rich stream. The main fermentation pathway was a propionate type since propionic acid raised up to 86.4% of total VFAs for the shortest HRT. The recirculation ratio still needs to be further investigated to deeper understand the influence on VFA productivity and composition. Despite the fact that dry AD is more prone to ammonia inhibition, the process achieved the maximum biogas production in terms of the gas production rate, which was 5.11 NL/(Lr d).

The next-generation sequencing analysis of the bacterial community increases the understanding of the complex microbial interactions in each section of the digester and the metabolic predominant pathways that alternatively operate the processes of transformation of the organic fractions, with the identification of relevant contributing taxa. Specifically, genus *Defluviitoga* sp. prevailed over other bacterial species along the digester, showing a bimodal distribution with two peaks at the entrance and at the outlet sections. The hydrolytic and acidogenic processes of proteins were clearly located in the central sections of the AD, in concomitance with propionate production increase, while hydrogen production during the acetogenic step might be spatially located before and after protein hydrolysis and fermentation, even if residual hydrogen at the end of the fermenter is neglectable. Predictive functional analysis of the bacterial community suggests that yet-unidentified species of the *Lentimicrobiaceae* family and *Proteiniphilum* are responsible for propionate production in the central sections of the reactor, while the genus *Defluviitoga* sp. hydrolyzes complex polysaccharides at the digester extremities.

Author Contributions: Conceptualization, E.R. and I.P.; methodology, E.R. and I.P.; software, S.B.; formal analysis, S.D.G. and I.P.; investigation, E.R., S.B. and I.P.; resources, I.P.; data curation, S.B. and E.R.; writing—original draft preparation, E.R. and S.B.; writing—review and editing, I.P., S.D.G.; visualization, E.R. and I.P.; supervision, I.P., S.D.G. and R.I.; project administration, I.P. and R.I.; funding acquisition, I.P. All authors have read and agreed to the published version of the manuscript.

Institutional Review Board Statement: Not applicable.

Informed Consent Statement: Not applicable.

Appendix A
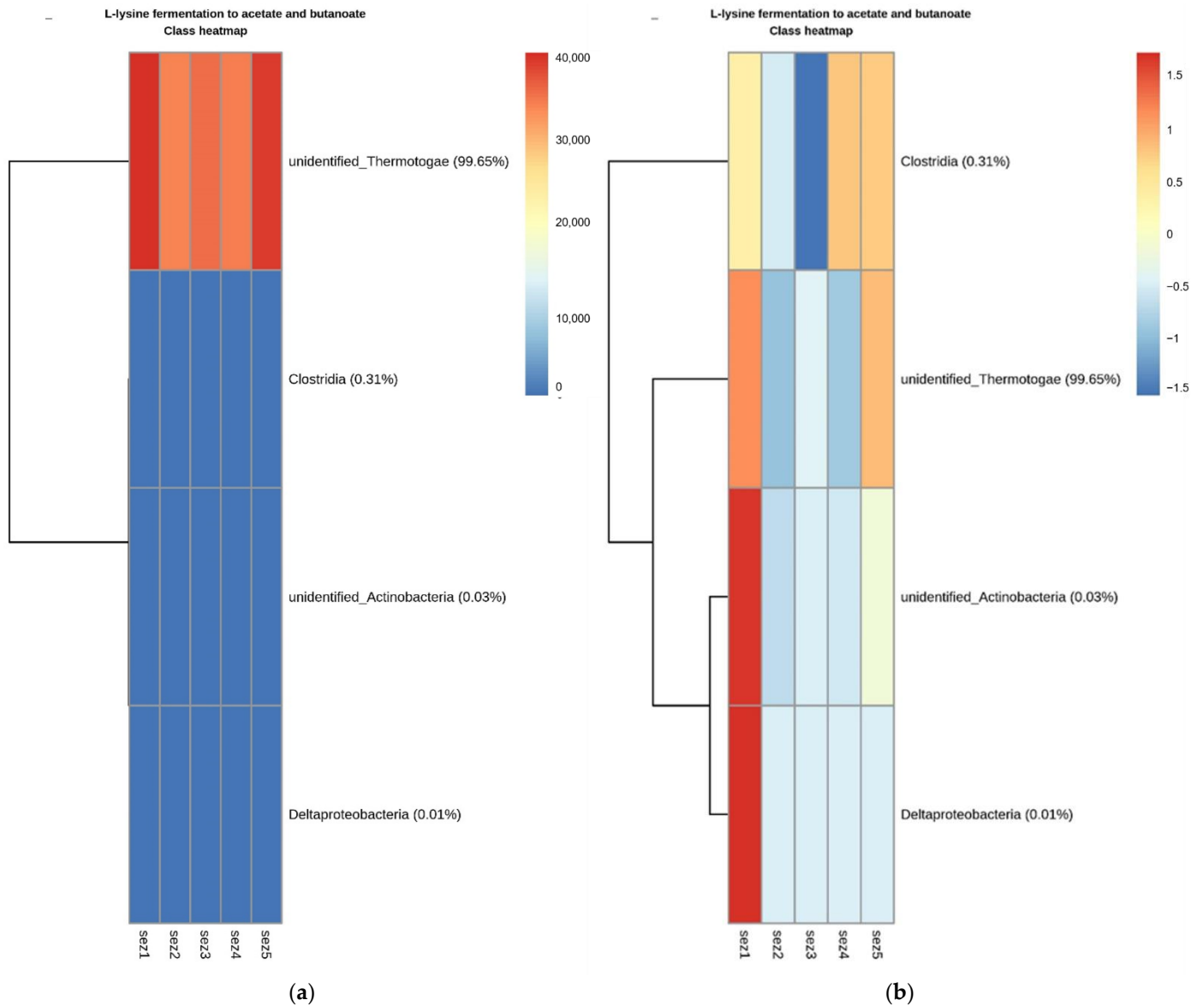
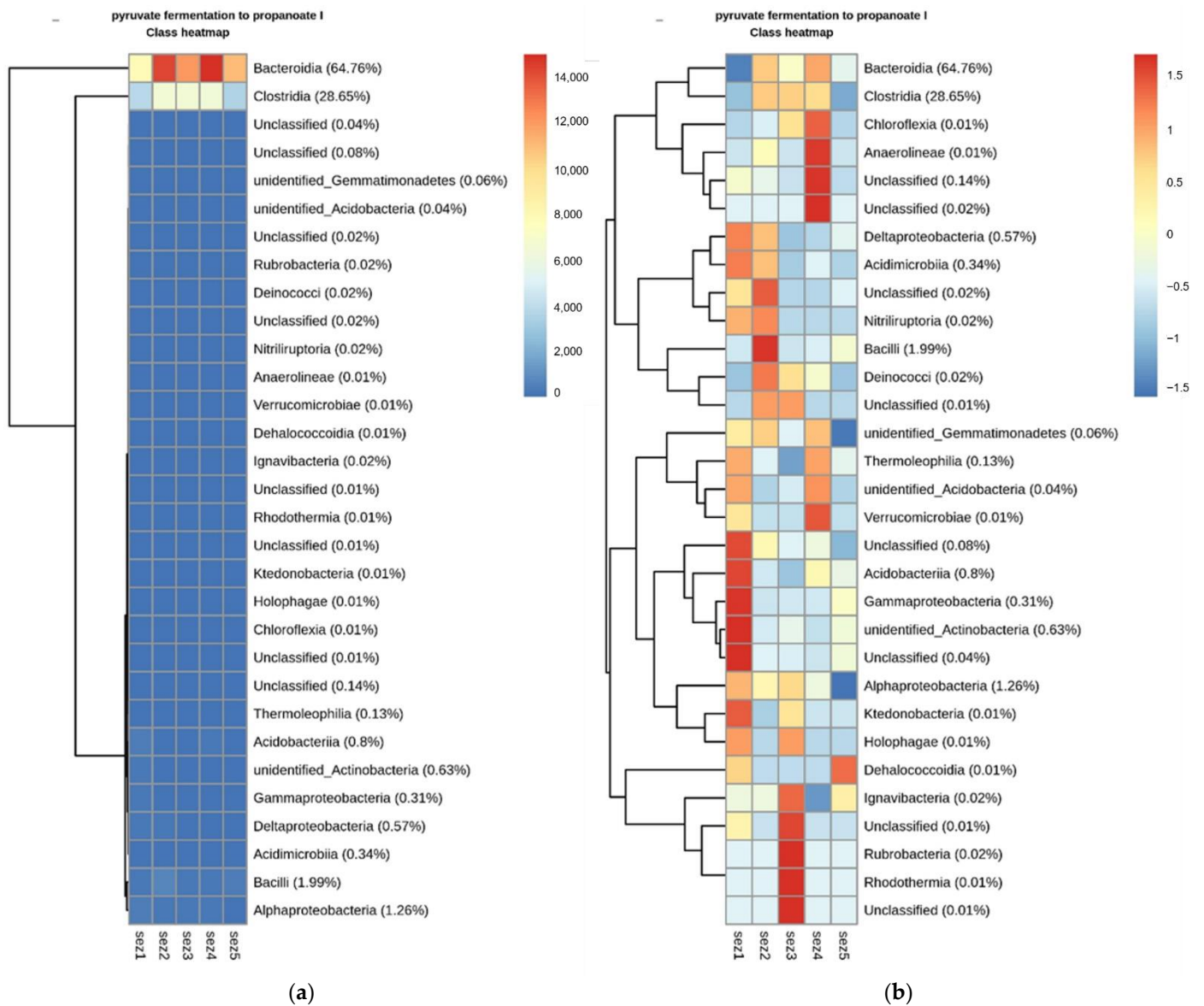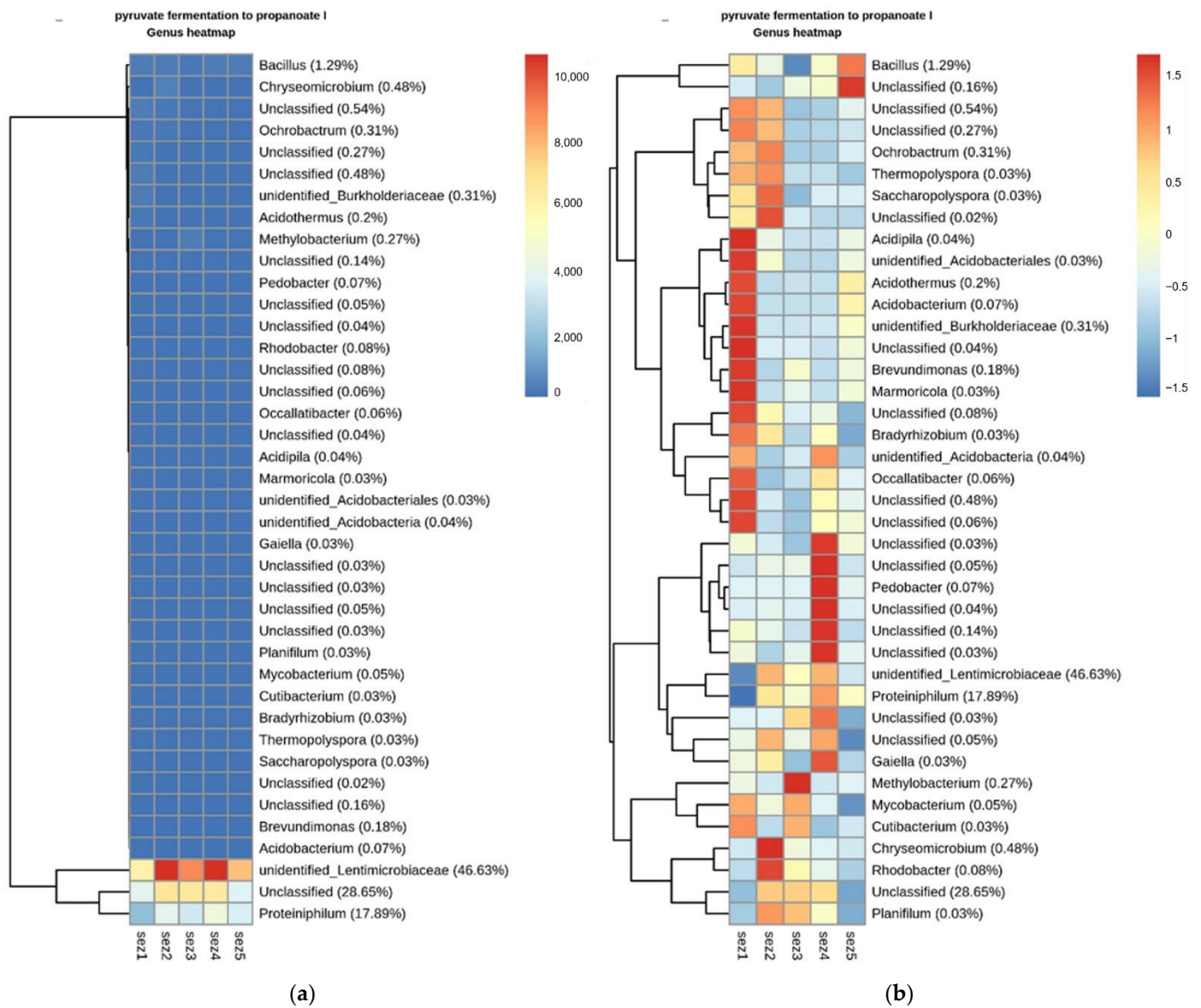**Figure A1.** Functional heatmaps of L-lysine fermentation to acetate and butanoate: (**a**) absolute counts and (**b**) autoscaled counts, aggregated at the class level.
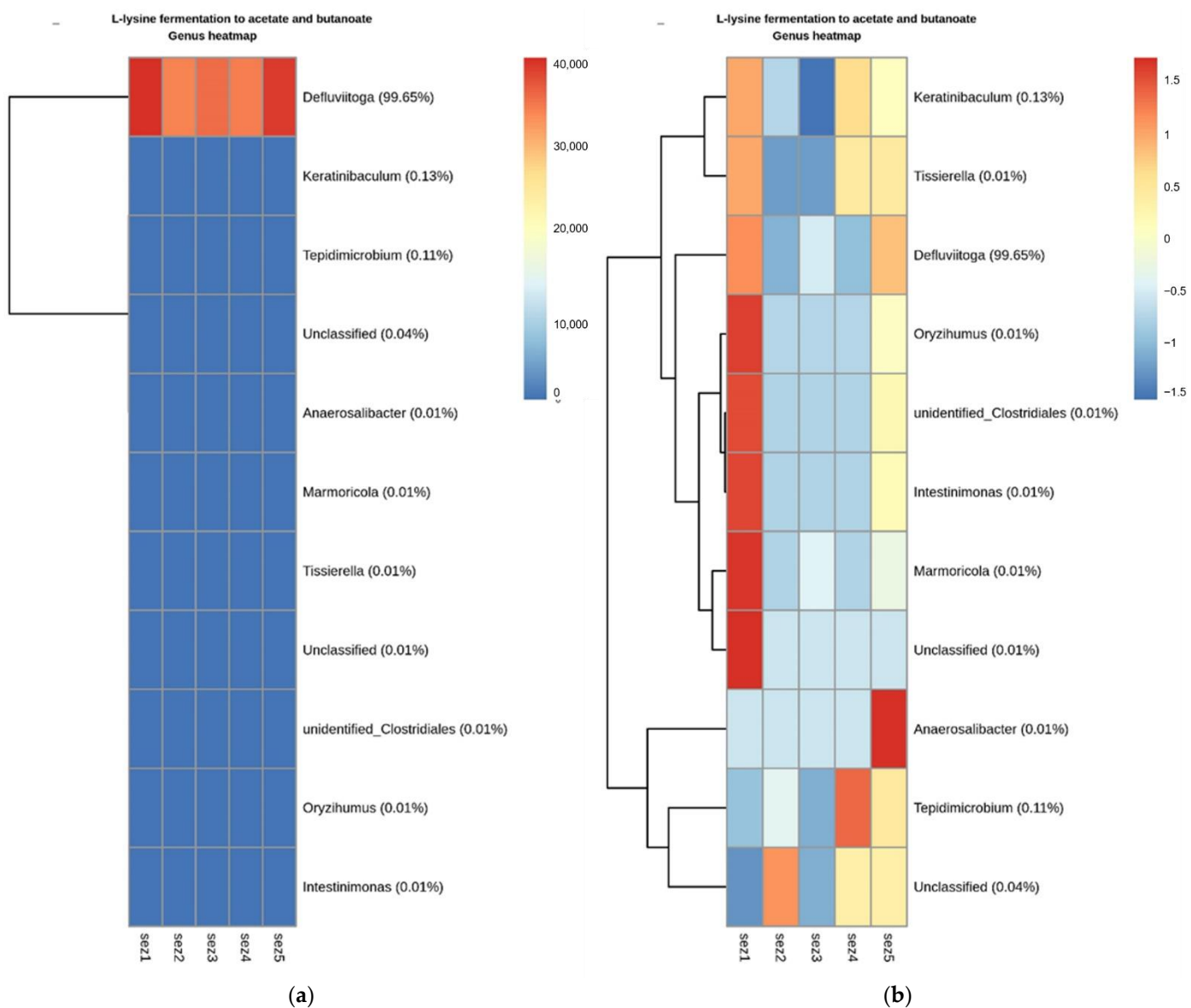
Figure A2. Functional heatmaps of L-lysine fermentation to acetate and butanoate: (**a**) absolute counts and (**b**) autoscaled counts, aggregated at the genus level.

Figure A3. Functional heatmaps of pyruvate fermentation to propanoate I: (**a**) absolute counts and (**b**) autoscaled counts, aggregated at the class level.
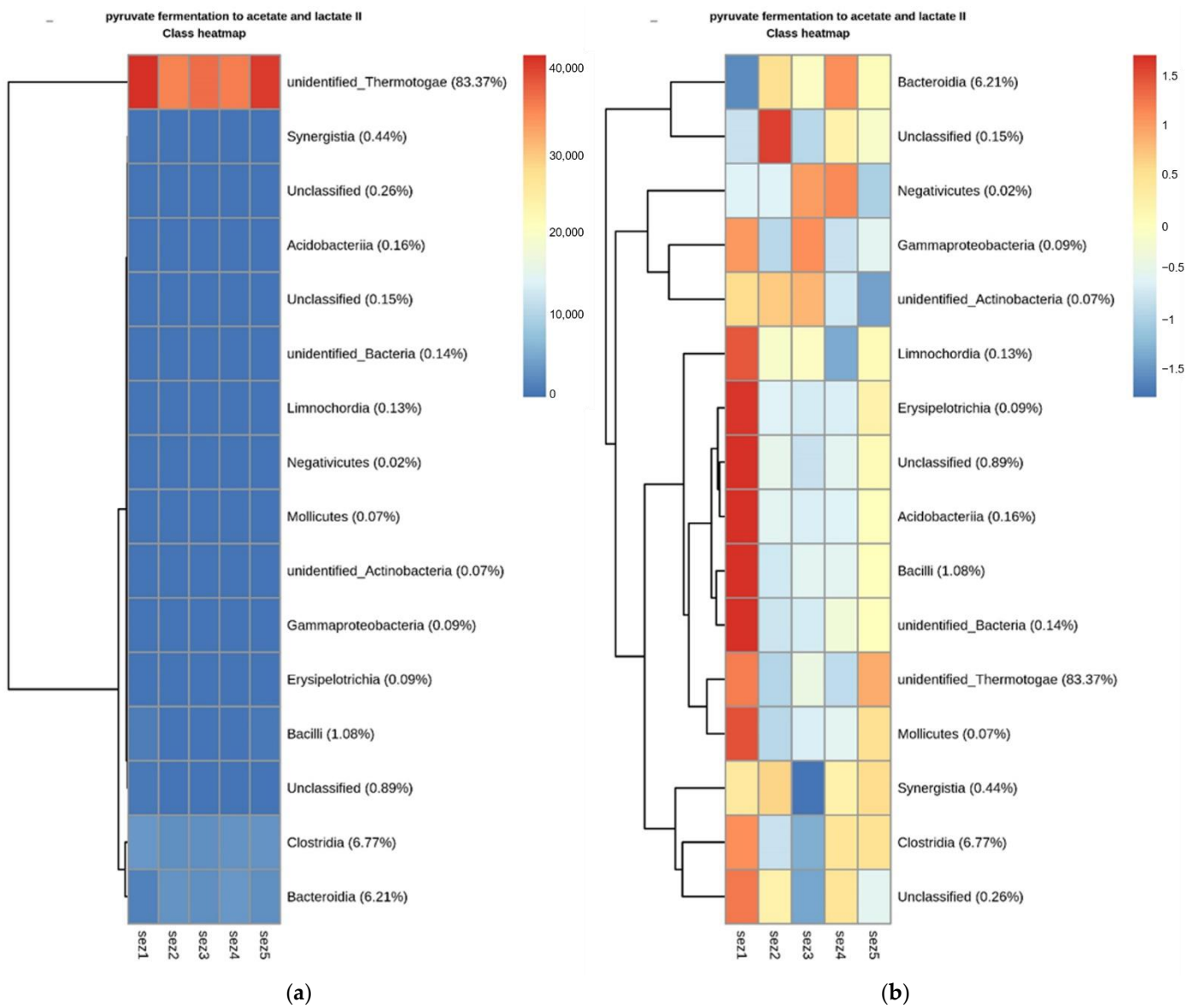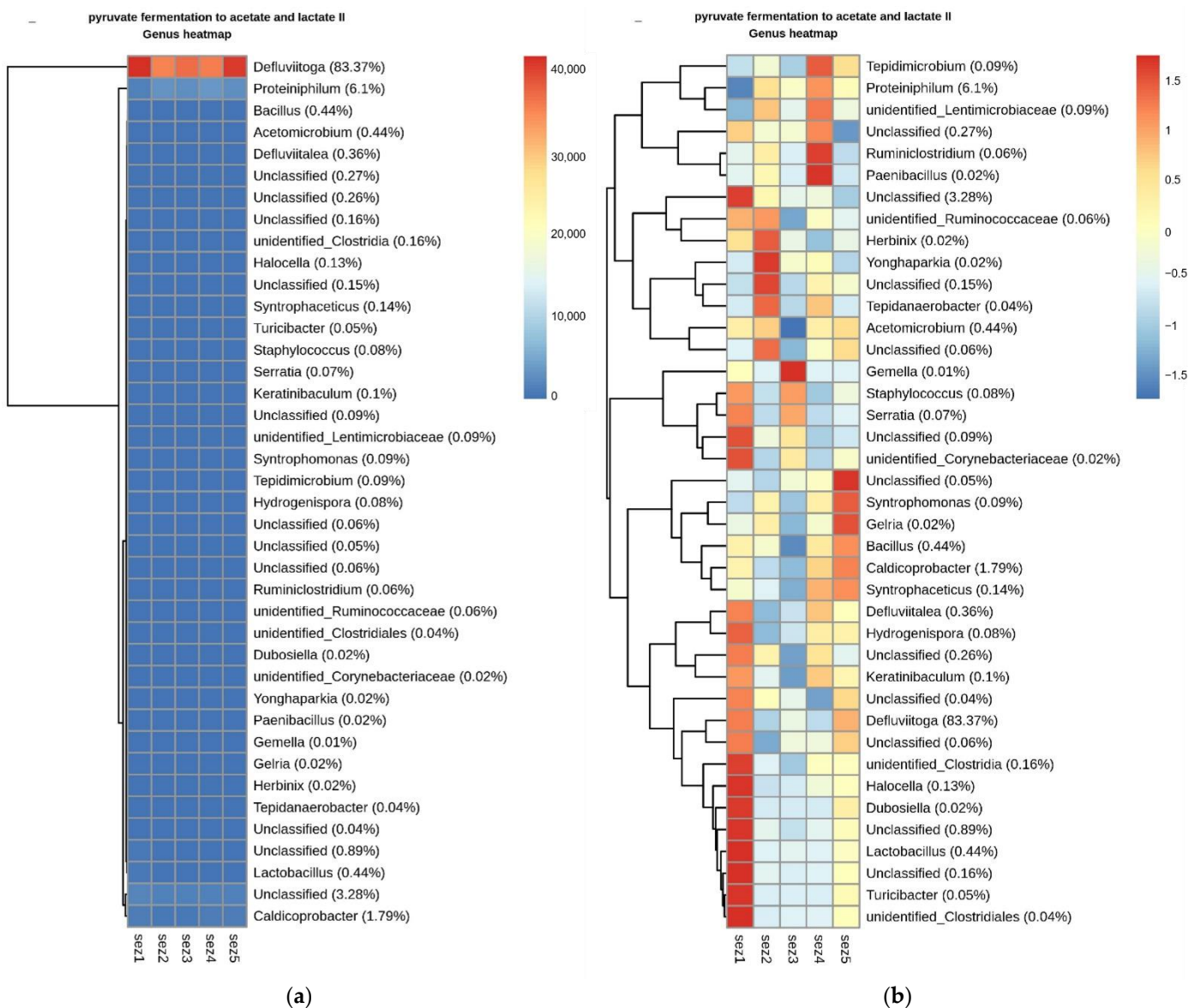
Figure A4. Functional heatmaps of pyruvate fermentation to propanoate I: (**a**) absolute counts and (**b**) autoscaled counts, aggregated at the genus level.

Figure A5. Functional heatmaps of pyruvate fermentation to acetate and lactate II: (**a**) absolute counts and (**b**) autoscaled counts, aggregated at the class level.
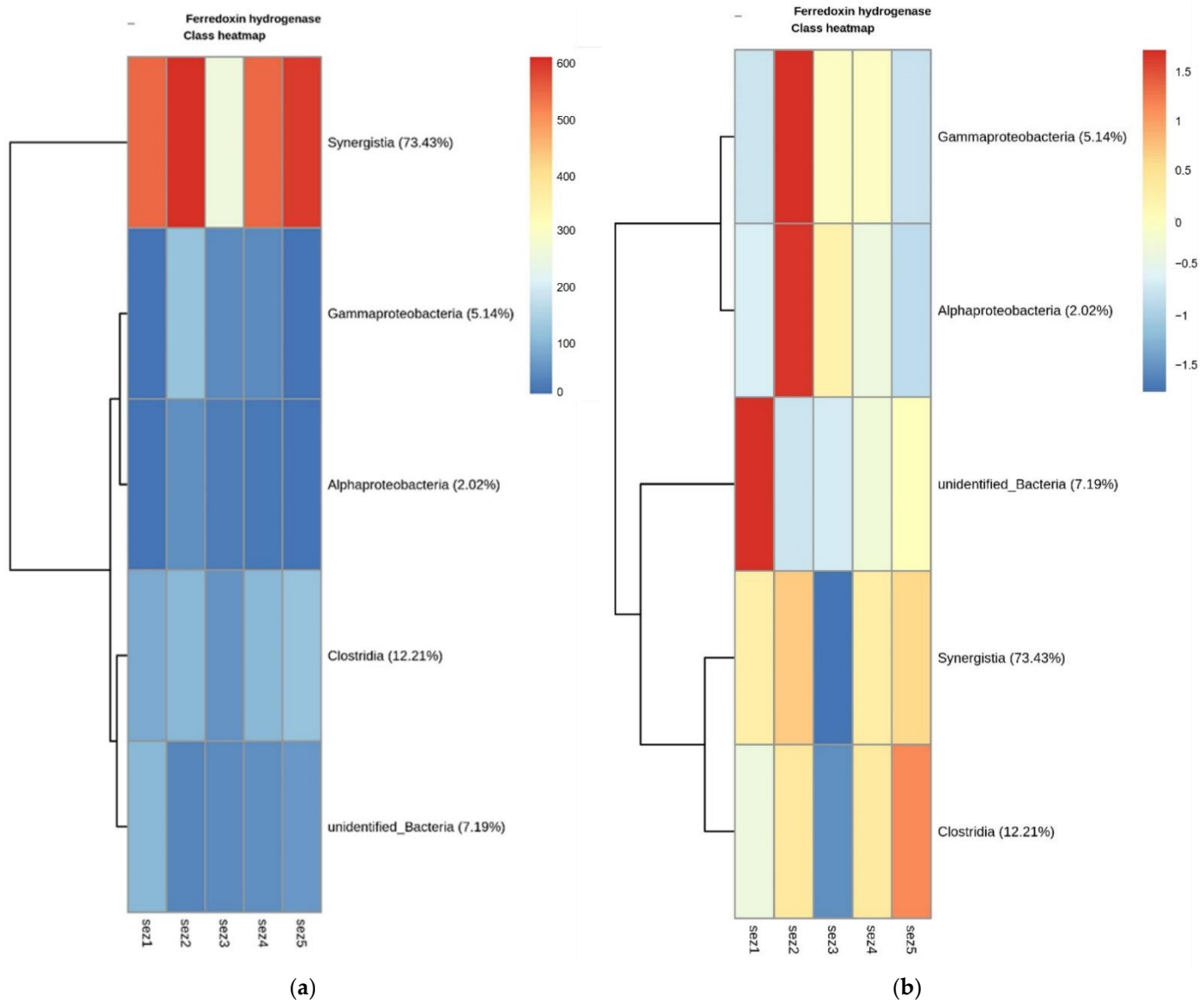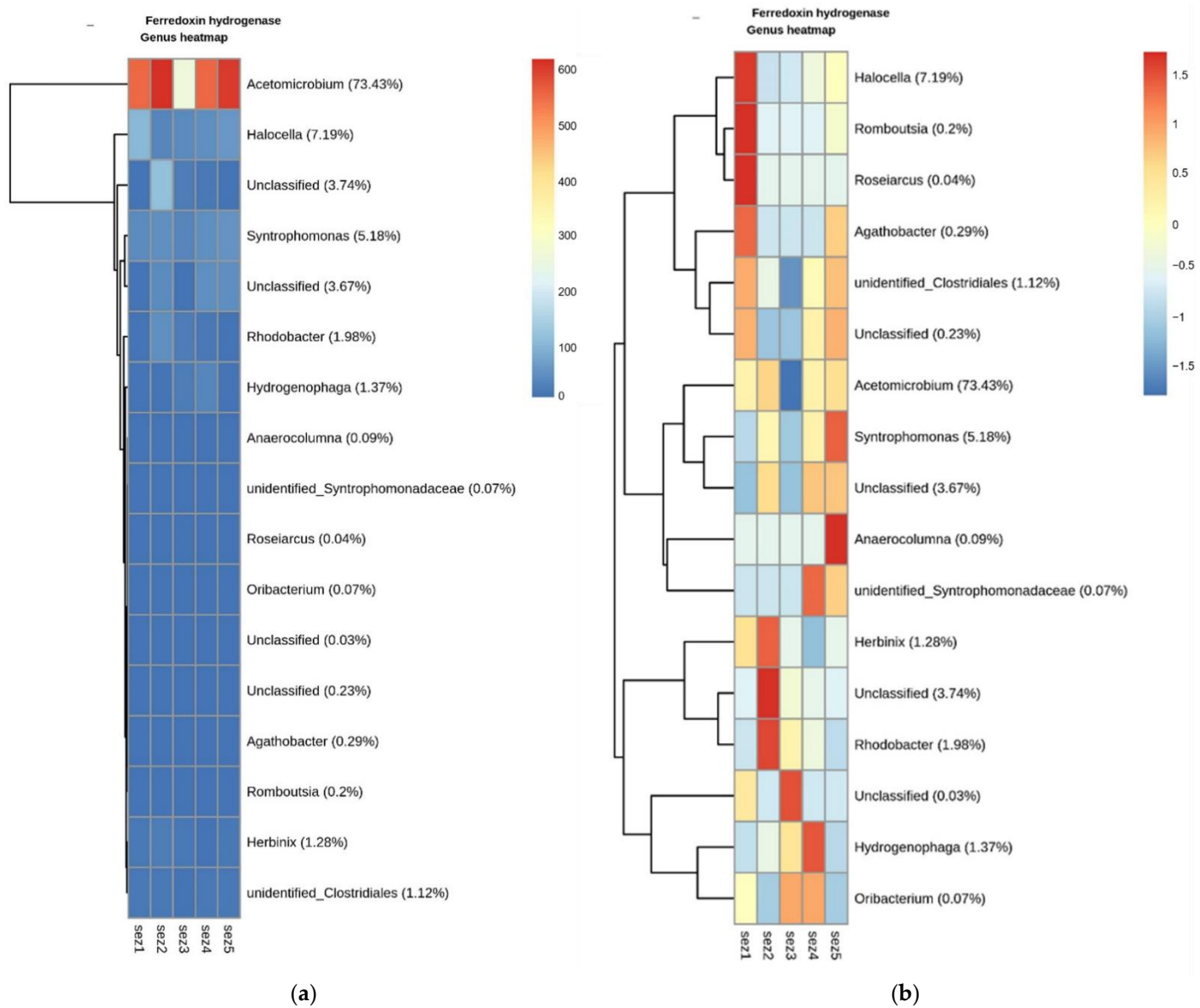
Figure A6. Functional heatmaps of pyruvate fermentation to acetate and lactate II: (**a**) absolute counts and (**b**) autoscaled counts, aggregated at the genus level.

Figure A7. Functional heatmaps of ferredoxin hydrogenase: (**a**) absolute counts and (**b**) autoscaled counts, aggregated at the class level.

Figure A8. Functional heatmaps of ferredoxin hydrogenase: (**a**) absolute counts and (**b**) autoscaled counts, aggregated at the genus level.
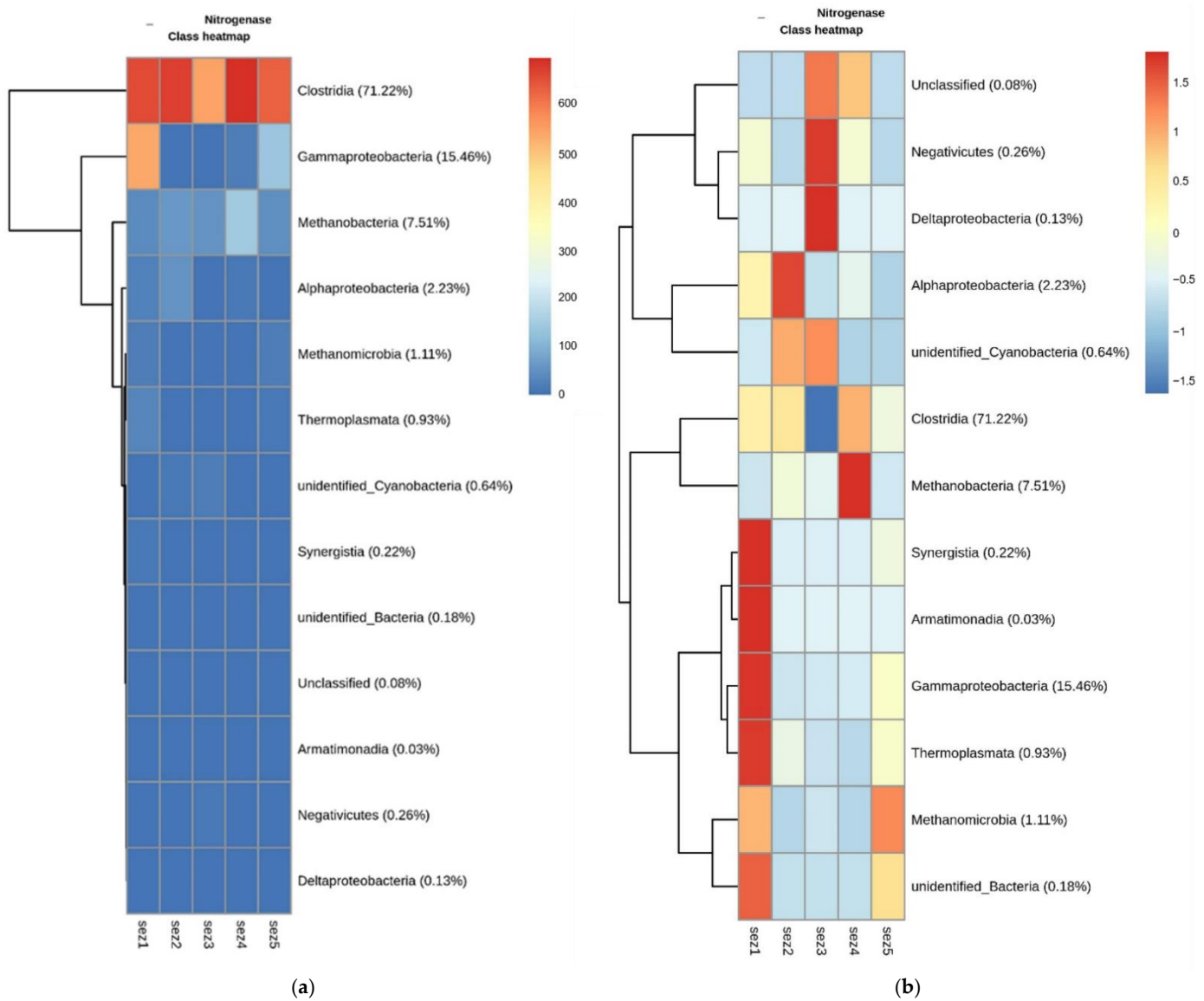
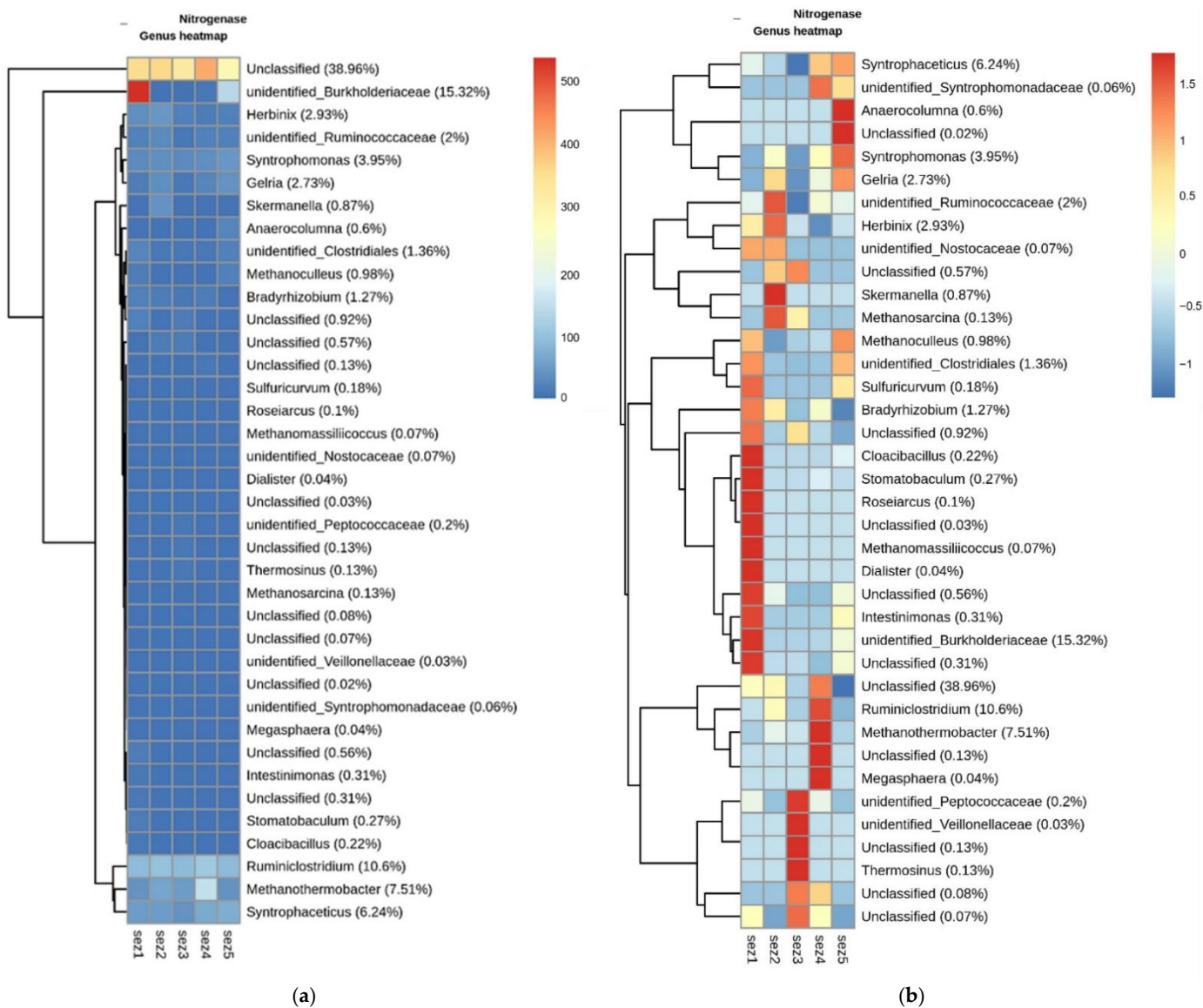**Figure A9.** Functional heatmaps of nitrogenase hydrogenase: (**a**) absolute counts and (**b**) autoscaled counts, aggregated at the class level.

Figure A10. Functional heatmaps of nitrogenase: (**a**) absolute counts and (**b**) autoscaled counts, aggregated at the genus level.

Appendix B

Table A1. The list of queried pathways.

MetaCyc Code	Pathway
2OXOBUTYRATECAT-PWY	2-oxobutanoate degradation II
PWY-5046	2-oxoisovalerate decarboxylation to isobutanoyl-CoA
PWY-5535	acetate formation from acetyl-CoA II
PWY-5536	acetate formation from acetyl-CoA III (succinate)
PWY-5676	acetyl-CoA fermentation to butanoate II
PWY0-43	conversion of succinate to propanoate
PROPFERM-PWY	L-alanine fermentation to propanoate and acetate
P162-PWY	L-glutamate degradation V (via hydroxyglutarate)
PWY-5088	L-glutamate degradation VIII (to propanoate)
PWY-5075	L-leucine degradation II
P163-PWY	L-lysine fermentation to acetate and butanoate
PWY-5096	pyruvate fermentation to acetate and alanine
P41-PWY	pyruvate fermentation to acetate and lactate I
PWY-5100	pyruvate fermentation to acetate and lactate II
P142-PWY	pyruvate fermentation to acetate I
PWY-5482	pyruvate fermentation to acetate II
PWY-5483	pyruvate fermentation to acetate III
PWY-5485	pyruvate fermentation to acetate IV
PWY-5538	pyruvate fermentation to acetate VI
PWY-5600	pyruvate fermentation to acetate VII
PWY-5768	pyruvate fermentation to acetate VIII
P108-PWY	pyruvate fermentation to propanoate I
PWY-5494	pyruvate fermentation to propanoate II (acrylate pathway)
PWY-5677	succinate fermentation to butanoate

References

1. European Commission Communication from the Commission to the European Parliament, the Council, the European Economic and Social Committee and the Committee of the Regions A new Circular Economy Action Plan for a Cleaner and More Competitive Europe. 2020. Available online: https://eur-lex.europa.eu/legal-content/EN/TXT/?qid=1583933814386&uri=COM:2020:98:FIN (accessed on 3 September 2021).
2. De Schoenmakere, M.; Hoogeveen, Y.; Gillabel, J.; Manshoven, S. European Environment Agency The Circular Economy and the Bioeconomy: Partners in Sustainability. Publications Office. 2018. Available online: https://data.europa.eu/doi/10.2800/00956 (accessed on 25 September 2021).
3. Council Directive (EU) 2018/851 of the European Parliament and of the Council of 30 May 2018 Amending Directive 2008/98/EC on Waste (Text with EEA Relevance); 2018; OJ L 150/109. Available online: https://eur-lex.europa.eu/eli/dir/2018/851/oj/eng (accessed on 4 November 2021).
4. Directive (EU) 2018/850 of the European Parliament and of the Council of 30 May 2018 Amending Directive 1999/31/EC on the Landfill of Waste (Text with EEA Relevance); 2018; OJ L 150/100. Available online: http://data.europa.eu/eli/dir/2018/850/oj/eng (accessed on 4 November 2021).
5. Strazzera, G.; Battista, F.; Garcia, N.H.; Frison, N.; Bolzonella, D. Volatile Fatty Acids Production from Food Wastes for Biorefinery Platforms: A Review. *J. Environ. Manag.* **2018**, *226*, 278–288. [CrossRef]
6. Ubando, A.T.; Felix, C.B.; Chen, W.-H. Biorefineries in Circular Bioeconomy: A Comprehensive Review. *Bioresour. Technol.* **2020**, *299*, 122585. [CrossRef]
7. Bhatia, S.K.; Yang, Y.-H. Microbial Production of Volatile Fatty Acids: Current Status and Future Perspectives. *Rev. Environ. Sci. Biotechnol.* **2017**, *16*, 327–345. [CrossRef]
8. Rocamora, I.; Wagland, S.T.; Villa, R.; Simpson, E.W.; Fernández, O.; Bajón-Fernández, Y. Dry Anaerobic Digestion of Organic Waste: A Review of Operational Parameters and Their Impact on Process Performance. *Bioresour. Technol.* **2020**, *299*, 122681. [CrossRef]
9. Karthikeyan, O.P.; Visvanathan, C. Bio-Energy Recovery from High-Solid Organic Substrates by Dry Anaerobic Bio-Conversion Processes: A Review. *Rev. Environ. Sci. Biotechnol.* **2013**, *12*, 257–284. [CrossRef]
10. Rosenheim, H.; De, I.; Hyvedemm, S. Anaerobic Digestion—Factsheet. 2015. Available online: https://docs.european-bioplastics.org/publications/bp/EUBP_BP_Anaerobic_digestion.pdf (accessed on 11 November 2021).
11. Mao, C.; Feng, Y.; Wang, X.; Ren, G. Review on Research Achievements of Biogas from Anaerobic Digestion. *Renew. Sustain. Energy Rev.* **2015**, *45*, 540–555. [CrossRef]

12. Karthikeyan, O.P.; Visvanathan, C. Effect of C/N Ratio and Ammonia-N Accumulation in a Pilot-Scale Thermophilic Dry Anaerobic Digester. *Bioresour. Technol.* **2012**, *113*, 294–302. [CrossRef]

13. Jabeen, M.; Zeshan; Yousaf, S.; Haider, M.R.; Malik, R.N. High-Solids Anaerobic Co-Digestion of Food Waste and Rice Husk at Different Organic Loading Rates. *Int. Biodeterior. Biodegrad.* **2015**, *102*, 149–153. [CrossRef]

14. Patinvoh, R.J.; Kalantar Mehrjerdi, A.; Sárvári Horváth, I.; Taherzadeh, M.J. Dry Fermentation of Manure with Straw in Continuous Plug Flow Reactor: Reactor Development and Process Stability at Different Loading Rates. *Bioresour. Technol.* **2017**, *224*, 197–205. [CrossRef]

15. Garcia-Aguirre, J.; Aymerich, E.; de Goñi, J.G.M.; Esteban-Gutiérrez, M. Selective VFA Production Potential from Organic Waste Streams: Assessing Temperature and PH Influence. *Bioresour. Technol.* **2017**, *244*, 1081–1088. [CrossRef] [PubMed]

16. Slezak, R.; Grzelak, J.; Krzystek, L.; Ledakowicz, S. The Effect of Initial Organic Load of the Kitchen Waste on the Production of VFA and H 2 in Dark Fermentation. *Waste Manag.* **2017**, *68*, 610–617. [CrossRef]

17. Wang, P.; Wang, H.; Qiu, Y.; Ren, L.; Jiang, B. Microbial Characteristics in Anaerobic Digestion Process of Food Waste for Methane Production—A Review. *Bioresour. Technol.* **2018**, *248*, 29–36. [CrossRef]

18. Khatami, K.; Atasoy, M.; Ludtke, M.; Baresel, C.; Eyice, Ö.; Cetecioglu, Z. Bioconversion of Food Waste to Volatile Fatty Acids: Impact of Microbial Community, PH and Retention Time. *Chemosphere* **2021**, *275*, 129981. [CrossRef] [PubMed]

19. Chen, R.; Li, Z.; Feng, J.; Zhao, L.; Yu, J. Effects of Digestate Recirculation Ratios on Biogas Production and Methane Yield of Continuous Dry Anaerobic Digestion. *Bioresour. Technol.* **2020**, *316*, 123963. [CrossRef]

20. Baldi, F.; Pecorini, I.; Iannelli, R. Comparison of Single-Stage and Two-Stage Anaerobic Co-Digestion of Food Waste and Activated Sludge for Hydrogen and Methane Production. *Renew. Energy* **2019**, *143*, 1755–1765. [CrossRef]

21. Angelidaki, I.; Alves, M.; Bolzonella, D.; Borzacconi, L.; Campos, J.L.; Guwy, A.J.; Kalyuzhnyi, S.; Jenicek, P.; van Lier, J.B. Defining the Biomethane Potential (BMP) of Solid Organic Wastes and Energy Crops: A Proposed Protocol for Batch Assays. *Water Sci. Technol.* **2009**, *59*, 927–934. [CrossRef] [PubMed]

22. Fagbohungbe, M.O.; Dodd, I.C.; Herbert, B.M.J.; Li, H.; Ricketts, L.; Semple, K.T. High Solid Anaerobic Digestion: Operational Challenges and Possibilities. *Environ. Technol. Innov.* **2015**, *4*, 268–284. [CrossRef]

23. Metcalf, N.A.; Eddy, I.; Tchobanoglous, G.; Burton, F.; Stensel, H.D. *Wastewater Engineering: Treatment and Reuse*; 4° Edizione; McGraw-Hill Education/Asia: Boston, MA, USA, 2002; ISBN 978-0-07-124140-3.

24. *Agenzia Nazionale per Protezione dell'Ambiente, Metodi di Analisi del Compost*; ANPA: Roma, Italy, 2001; ISBN 88-448-0258-9.

25. Ripley, L.E.; Boyle, W.C.; Converse, J.C. Improved Alkalimetric Monitoring for Anaerobic Digestion of High-Strength Wastes. *J. Water Pollut. Control Fed.* **1986**, *58*, 406–411.

26. Drosg, B. Process Monitoring in Biogas Plants. 40. Available online: https://www.ieabioenergy.com/wp-content/uploads/2013/12/Technical-Brochure-process_montoring.pdf (accessed on 16 October 2021).

27. Rajagopal, R.; Massé, D.I.; Singh, G. A Critical Review on Inhibition of Anaerobic Digestion Process by Excess Ammonia. *Bioresour. Technol.* **2013**, *143*, 632–641. [CrossRef]

28. Baldi, F.; Iannelli, R.; Pecorini, I.; Polettini, A.; Pomi, R.; Rossi, A. Influence of the PH Control Strategy and Reactor Volume on Batch Fermentative Hydrogen Production from the Organic Fraction of Municipal Solid Waste. *Waste Manag. Res.* **2019**, *37*, 478–485. [CrossRef]

29. Kothari, R.; Pandey, A.K.; Kumar, S.; Tyagi, V.V.; Tyagi, S.K. Different Aspects of Dry Anaerobic Digestion for Bio-Energy: An Overview. *Renew. Sustain. Energy Rev.* **2014**, *39*, 174–195. [CrossRef]

30. Microbiome Informatics: OTU vs. ASV. Available online: https://www.zymoresearch.com/blogs/blog/microbiome-informatics-otu-vs-asv (accessed on 6 December 2021).

31. Sikora, A.; Detman, A.; Mielecki, D.; Chojnacka, A.; Błaszczyk, M. *Searching for Metabolic Pathways of Anaerobic Digestion: A Useful List of the Key Enzymes*; IntechOpen: London, UK, 2018; ISBN 978-1-83881-850-0.

32. Wiechmann, A.; Ciurus, S.; Oswald, F.; Seiler, V.N.; Müller, V. It Does Not Always Take Two to Tango: "Syntrophy" via Hydrogen Cycling in One Bacterial Cell. *ISME J.* **2020**, *14*, 1561–1570. [CrossRef]

33. Lee, W.S.; Chua, A.S.M.; Yeoh, H.K.; Ngoh, G.C. A Review of the Production and Applications of Waste-Derived Volatile Fatty Acids. *Chem. Eng. J.* **2014**, *235*, 83–99. [CrossRef]

34. Zhou, M.; Yan, B.; Wong, J.W.C.; Zhang, Y. Enhanced Volatile Fatty Acids Production from Anaerobic Fermentation of Food Waste: A Mini-Review Focusing on Acidogenic Metabolic Pathways. *Bioresour. Technol.* **2018**, *248*, 68–78. [CrossRef] [PubMed]

35. Li, L.; Qin, Y.; Kong, Z.; Wu, J.; Kubota, K.; Li, Y.-Y. Characterization of Microbial Community and Main Functional Groups of Prokaryotes in Thermophilic Anaerobic Co-Digestion of Food Waste and Paper Waste. *Sci. Total Environ.* **2019**, *652*, 709–717. [CrossRef] [PubMed]

36. Guo, X.; Wang, C.; Sun, F.; Zhu, W.; Wu, W. A Comparison of Microbial Characteristics between the Thermophilic and Mesophilic Anaerobic Digesters Exposed to Elevated Food Waste Loadings. *Bioresour. Technol.* **2014**, *152*, 420–428. [CrossRef]

37. Dyksma, S.; Jansen, L.; Gallert, C. Syntrophic Acetate Oxidation Replaces Acetoclastic Methanogenesis during Thermophilic Digestion of Biowaste. *Microbiome* **2020**, *8*, 105. [CrossRef]

38. Fernández-Domínguez, D.; Astals, S.; Peces, M.; Frison, N.; Bolzonella, D.; Mata-Alvarez, J.; Dosta, J. Volatile Fatty Acids Production from Biowaste at Mechanical-Biological Treatment Plants: Focusing on Fermentation Temperature. *Bioresour. Technol.* **2020**, *314*, 123729. [CrossRef]

39. Campuzano, R.; González-Martínez, S. Characteristics of the Organic Fraction of Municipal Solid Waste and Methane Production: A Review. *Waste Manag.* **2016**, *54*, 3–12. [CrossRef]

40. Garcia-Aguirre, J.; Esteban-Gutiérrez, M.; Irizar, I.; González-Mtnez de Goñi, J.; Aymerich, E. Continuous Acidogenic Fermentation: Narrowing the Gap between Laboratory Testing and Industrial Application. *Bioresour. Technol.* **2019**, *282*, 407–416. [CrossRef]

41. Papa, G.; Pepè Sciarria, T.; Carrara, A.; Scaglia, B.; D'Imporzano, G.; Adani, F. Implementing Polyhydroxyalkanoates Production to Anaerobic Digestion of Organic Fraction of Municipal Solid Waste to Diversify Products and Increase Total Energy Recovery. *Bioresour. Technol.* **2020**, *318*, 124270. [CrossRef] [PubMed]

42. Esteban-Gutiérrez, M.; Garcia-Aguirre, J.; Irizar, I.; Aymerich, E. From Sewage Sludge and Agri-Food Waste to VFA: Individual Acid Production Potential and up-Scaling. *Waste Manag.* **2018**, *77*, 203–212. [CrossRef]

43. Yoo, C.G.; Meng, X.; Pu, Y.; Ragauskas, A.J. The Critical Role of Lignin in Lignocellulosic Biomass Conversion and Recent Pretreatment Strategies: A Comprehensive Review. *Bioresour. Technol.* **2020**, *301*, 122784. [CrossRef]

44. Chen, Y.; Cheng, J.J.; Creamer, K.S. Inhibition of Anaerobic Digestion Process: A Review. *Bioresour. Technol.* **2008**, *99*, 4044–4064. [CrossRef]

45. Liu, T.; Schnürer, A.; Björkmalm, J.; Willquist, K.; Kreuger, E. Diversity and Abundance of Microbial Communities in UASB Reactors during Methane Production from Hydrolyzed Wheat Straw and Lucerne. *Microorganisms* **2020**, *8*, 1394. [CrossRef] [PubMed]

46. Zhao, J.; Li, Y.; Marandola, C.; Krooneman, J.; Euverink, G.J.W. Comparison of the Microbial Communities in Anaerobic Digesters Treating High Alkalinity Synthetic Wastewater at Atmospheric and High-Pressure (11 Bar). *Bioresour. Technol.* **2020**, *318*, 124101. [CrossRef]

47. Svensson, K.; Paruch, L.; Gaby, J.C.; Linjordet, R. Feeding Frequency Influences Process Performance and Microbial Community Composition in Anaerobic Digesters Treating Steam Exploded Food Waste. *Bioresour. Technol.* **2018**, *269*, 276–284. [CrossRef] [PubMed]

48. Ao, T.; Xie, Z.; Zhou, P.; Liu, X.; Wan, L.; Li, D. Comparison of Functional Microbial Profile between Mesophilic and Thermophilic Anaerobic Digestion of Vegetable Waste. 2021. Available online: https://www.researchsquare.com/article/rs-54152/v1 (accessed on 18 October 2021).

49. Jang, H.M.; Ha, J.H.; Kim, M.-S.; Kim, J.-O.; Kim, Y.M.; Park, J.M. Effect of Increased Load of High-Strength Food Wastewater in Thermophilic and Mesophilic Anaerobic Co-Digestion of Waste Activated Sludge on Bacterial Community Structure. *Water Res.* **2016**, *99*, 140–148. [CrossRef]

50. Maus, I.; Cibis, K.G.; Bremges, A.; Stolze, Y.; Wibberg, D.; Tomazetto, G.; Blom, J.; Sczyrba, A.; König, H.; Pühler, A.; et al. Genomic Characterization of *Defluviitoga tunisiensis* L3, a Key Hydrolytic Bacterium in a Thermophilic Biogas Plant and Its Abundance as Determined by Metagenome Fragment Recruitment. *J. Biotechnol.* **2016**, *232*, 50–60. [CrossRef]

51. Sun, L.; Toyonaga, M.; Ohashi, A.; Tourlousse, D.M.; Matsuura, N.; Meng, X.-Y.; Tamaki, H.; Hanada, S.; Cruz, R.; Yamaguchi, T.; et al. *Lentimicrobium saccharophilum* Gen. Nov., Sp. Nov., a Strictly Anaerobic Bacterium Representing a New Family in the Phylum *Bacteroidetes*, and Proposal of *Lentimicrobiaceae* Fam. Nov. *Int. J. Syst. Evol. Microbiol.* **2016**, *66*, 2635–2642. [CrossRef]

52. Chen, S.; Dong, X. *Proteiniphilum acetatigenes* Gen. Nov., Sp. Nov., from a UASB Reactor Treating Brewery Wastewater. *Int. J. Syst. Evol. Microbiol.* **2005**, *55*, 2257–2261. [CrossRef] [PubMed]

53. Tomazetto, G.; Hahnke, S.; Wibberg, D.; Pühler, A.; Klocke, M.; Schlüter, A. *Proteiniphilum saccharofermentans* Str. M3/6T Isolated from a Laboratory Biogas Reactor Is Versatile in Polysaccharide and Oligopeptide Utilization as Deduced from Genome-Based Metabolic Reconstructions. *Biotechnol. Rep.* **2018**, *18*, e00254. [CrossRef]

54. Breure, A.M.; Mooijman, K.A.; van Andel, J.G. Protein Degradation in Anaerobic Digestion: Influence of Volatile Fatty Acids and Carbohydrates on Hydrolysis and Acidogenic Fermentation of Gelatin. *Appl. Microbiol. Biotechnol.* **1986**, *24*, 426–431. [CrossRef]

55. Bouanane-Darenfed, A.; Ben Hania, W.; Cayol, J.-L.; Ollivier, B.; Fardeau, M.-L. Reclassification of *Acetomicrobium faecale* as *Caldicoprobacter faecalis* Comb. Nov. *Int. J. Syst. Evol. Microbiol.* **2015**, *65*, 3286–3288. [CrossRef]

56. Hazlewood, G.P.; Gilbert, H.J. Xylan and Cellulose Utilization by the Clostridia. *Biotechnol. Read. Mass* **1993**, *25*, 311–341.

57. Fonknechten, N.; Chaussonnerie, S.; Tricot, S.; Lajus, A.; Andreesen, J.R.; Perchat, N.; Pelletier, E.; Gouyvenoux, M.; Barbe, V.; Salanoubat, M.; et al. *Clostridium sticklandii*, a Specialist in Amino Acid Degradation:Revisiting Its Metabolism through Its Genome Sequence. *BMC Genom.* **2010**, *11*, 555. [CrossRef]

58. Park, G.W.; Kim, I.; Jung, K.; Seo, C.; Han, J.-I.; Chang, H.N.; Kim, Y.-C. Enhancement of Volatile Fatty Acids Production from Rice Straw via Anaerobic Digestion with Chemical Pretreatment. *Bioprocess Biosyst. Eng.* **2015**, *38*, 1623–1627. [CrossRef]

59. Smith, E.A.; Macfarlane, G.T. Enumeration of Amino Acid Fermenting Bacteria in the Human Large Intestine: Effects of PH and Starch on Peptide Metabolism and Dissimilation of Amino Acids. *FEMS Microbiol. Ecol.* **1998**, *25*, 355–368. [CrossRef]

60. Westerholm, M.; Roos, S.; Schnürer, A. *Syntrophaceticus schinkii* Gen. Nov., Sp. Nov., an Anaerobic, Syntrophic Acetate-Oxidizing Bacterium Isolated from a Mesophilic Anaerobic Filter. *FEMS Microbiol. Lett.* **2010**, *309*, 100–104. [CrossRef]

61. Wainaina, S.; Lukitawesa; Kumar Awasthi, M.; Taherzadeh, M.J. Bioengineering of Anaerobic Digestion for Volatile Fatty Acids, Hydrogen or Methane Production: A Critical Review. *Bioengineered* **2019**, *10*, 437–458. [CrossRef]

62. Amha, Y.M.; Anwar, M.Z.; Brower, A.; Jacobsen, C.S.; Stadler, L.B.; Webster, T.M.; Smith, A.L. Inhibition of Anaerobic Digestion Processes: Applications of Molecular Tools. *Bioresour. Technol.* **2018**, *247*, 999–1014. [CrossRef] [PubMed]

63. Einsle, O.; Rees, D.C. Structural Enzymology of Nitrogenase Enzymes. *Chem. Rev.* **2020**, *120*, 4969–5004. [CrossRef] [PubMed]

64. Artz, J.H.; Zadvornyy, O.A.; Mulder, D.W.; Keable, S.M.; Cohen, A.E.; Ratzloff, M.W.; Williams, S.G.; Ginovska, B.; Kumar, N.; Song, J.; et al. Tuning Catalytic Bias of Hydrogen Gas Producing Hydrogenases. *J. Am. Chem. Soc.* **2020**, *142*, 1227–1235. [CrossRef]

65. Sokolova, T.G.; Henstra, A.-M.; Sipma, J.; Parshina, S.N.; Stams, A.J.M.; Lebedinsky, A.V. Diversity and Ecophysiological Features of Thermophilic Carboxydotrophic Anaerobes: Thermophilic Carboxydotrophic Anaerobes. *FEMS Microbiol. Ecol.* **2009**, *68*, 131–141. [CrossRef] [PubMed]